


Article

Stochastic Modeling of Chemical Compounds in a Limestone Deposit by Unlocking the Complexity in Bivariate Relationships

Nurassyl Battalgazy and Nasser Madani * 

School of Mining and Geosciences, Nazarbayev University, Nur-Sultan 010000, Kazakhstan;
nurassyl.battalgazy@nu.edu.kz

* Correspondence: nasser.madani@nu.edu.kz; Tel.: +7-747-1755327

Received: 12 October 2019; Accepted: 2 November 2019; Published: 4 November 2019



Abstract: Modeling multivariate variables with complexity in a cross-correlation structure is always applicable to mineral resource evaluation and exploration in multi-element deposits. However, the geostatistical algorithm for such modeling is usually challenging. In this respect, projection pursuit multivariate transform (PPMT), which can successfully handle the complexity of interest in bivariate relationships, may be particularly useful. This work presents an algorithm for combining projection pursuit multivariate transform (PPMT) with a conventional (co)-simulation technique where spatial dependency among variables can be defined by a linear model of co-regionalization (LMC). This algorithm is examined by one real case study in a limestone deposit in the south of Kazakhstan, in which four chemical compounds (CaO , Al_2O_3 , Fe_2O_3 , and SiO_2) with complexity in bivariate relationships are analyzed and 100 realizations are produced for each variable. To show the effectiveness of the proposed algorithm, the outputs (realizations) are statistically examined and the results show that this methodology is legitimate for reproduction of original mean, variance, and complex cross-correlation among the variables and can be employed for further processes. Then, the applicability of the concept is demonstrated on a workflow to classify this limestone deposit as measured, indicated, or inferred based on Joint Ore Reserves Committee (JORC) code. The categorization is carried out based on two zone definitions, geological, and mining units.

Keywords: mineral resource classification; JORC code; limestone deposit; project pursuit multivariate transform; (co)-simulation

1. Introduction

Accurate evaluation of viable mineral resources is fundamentally important in optimal sustainable development and mine planning procedures since it has an enormous impact on the value of produced metals and formation of technical plans, from extraction to closure of the mine [1–3]. In the world of emerging new technologies and increasing complexity for modeling the grades and chemical compounds in deposits, precise estimation and classification of resources is becoming more crucial, as it can vary depending on the technological modifications that change the notion of mine planning [4]. Nowadays, the “best practice” in resource classification takes into account assumptions made in grades and tonnages of orebodies, as well as in the methods applied, future expenses, and commodity costs. One of the main ways to solve these issues is to consider uncertainty and risk assessment [5–7]. Consequently, integrating enhanced geostatistical techniques in order to quantify uncertainty in the process of evaluating resources allow practitioners to effectively unlock the complexity in the modeling of mineral deposits [8,9].

In every mining project, the discrepancy between the estimated resource model and actual production value is the main concern, which leads to low probability of meeting production targets

in respect to quality and quantity of ore content, which can be stated as unsuccessful operation of the mine [10]. In this respect, resource estimation basically depends on the block model, which can be constructed by different deterministic and stochastic approaches. Commonly, the procedure of resource estimation and classification is done on the basis of a block model of a deposit, in which it can be constructed by conventional (deterministic) methods of geostatistics such as kriging. This type of linear interpolation method provides only one unique scenario from a deposit [11] that, in fact, is inadequate to represent the variable under study, with a direct impact on further steps of a mining project, including determining optimum pit shell for scheduling, identifying the sequence of the block extraction intended to generate the best Net Present Value (NPV), and projecting the pushbacks (phases of the mine) [1]. Hence, the main problems in conventional methods not only affect the poor reproduction of original variability of grade (e.g., smoothing effect), but also lead to other issues such as the inability to quantify the uncertainty within each block. Ignoring this type of valuable information, such as risk and uncertainty, in mineral resource evaluation may result in unrealistic outcomes of planned production and cash flow of mine projects [10,12]. The existence of uncertainties in the block model and other parameters makes consideration of a single deterministic model doubtful for resource classification [13]. In contrast, the application of stochastic models to the estimation of resources based on international standards is important in terms of both reproducing original variability of grade and quantifying uncertainty [14]. In this regard, there are two commonly used simulation methods, turning bands (co)-simulation [15] and sequential Gaussian (co)-simulation [16,17]. However, these approaches are restricted to the linear bivariate characteristics among the variables and are insufficient to properly handle the orebodies wherever complexities such as heteroscedasticity, nonlinearity, and geological constraints in cross-correlation structures inherently exist [18,19]. To address these complexities, another geostatistical approach, such as stepwise conditioning transformation (SCT) [20], flow anamorphosis [21], or projection pursuit multivariate transform [22,23], can be an option for unlocking the complexity among the variables. The latter honors the complex multivariate normality after transformation and allows back-transformation of the simulated variables to the original dataset as well as restoring the multivariate characteristics [24,25]. Applications of PPMT in 3D multivariate geosciences mapping include petroleum reservoirs [23], environmental studies [26], grade control [27], and mineral resource classification [24]. However, PPMT, in some circumstances, does not completely remove the cross-dependency among the variables, and PPMT forward transformation may show some slight dependency [21] in bivariate relationships. In order to circumvent this impediment, one more step of factorization with a technique such as minimum/maximum autocorrelation factor (MAF) can be applied to make sure the correlation is removed not only in lag 0, but also in other arbitrary lag. However, MAF may not be enough to eliminate the correlation at lags other than these two lag separations. In this study, we propose an approach that is a combination of PPMT and (co)-simulation techniques. This takes into account the linear model of co-regionalization for defining cross-spatial dependency in order to establish the (co)-kriging system in the (co)-simulation algorithm right after transforming multivariate variables to PPMT factors. In the proposed algorithm, it is not necessary to employ MAF or any other factorization technique for further decorrelation.

The discussion of this paper is thus relevant for multivariate analysis of any complex bivariate features and can be applied to many cases.

The objectives of this paper are fourfold: (1) to briefly present the concept of (co)-simulation and PPMT and the proposed algorithm; (2) to apply the proposed algorithm in a real case study of a limestone deposit in Kazakhstan; (3) to classify resources based on Joint Ore Reserves Committee (JORC) code over the results obtained for objective 2; and (4) to provide a discussion and conclusion.

2. Methodology

2.1. Gaussian (Co)-Simulation

Stochastic simulation requires the transformation of variables into normal score values with zero mean and variance equal to 1. Generally, the transformation can be executed through Gaussian

anamorphosis, which transforms variables into standard Gaussian form [28], or a quantile–quantile based approach [29]. With two or more variables, multivariable geostatistical modelling is based on the multivariate Gaussianity assumption [16,30]. In this technique, the variables should be independently transferred to normal Gaussian distribution. Then, (co)-simulation can be performed over normal score data, taking into account the cross-dependency functions that are defined by, for instance, a linear model of co-regionalization. The obtained realizations can subsequently be back-transformed to original scale in order to approximately reproduce the original linear multivariate relationships among the variables. Despite the fact that independent normal score transform ensures that each item of normal score data is multi-Gaussian, the multivariate Gaussianity assumption is violated when there is complexity in bivariate relations between pairs of variables. For example, with features such as geological constraints, heteroscedasticity, and nonlinearity, as illustrated in Figure 1 [31], that employ the typical (co)-simulation algorithm, using the multi-Gaussianity assumption is problematic. In other words, in a typical (co)-simulation paradigm, in order to implement the algorithms effectively, the normal score transformed data should follow the elliptical (Figure 1a). However, in the case of nonlinearity, heteroscedasticity, or linearity constraints (Figure 1), the multi-Gaussianity assumption cannot be respected and the outputs of typical (co)-simulation algorithms are unsatisfactory. To cope with this difficulty, one idea is to use another transformation technique such as projection pursuit multivariate transformation (PPMT) [23,24] rather than the regular normal score transformation (e.g., quantile–quantile or Gaussian anamorphosis [28,29]) that is common for univariate transformation.

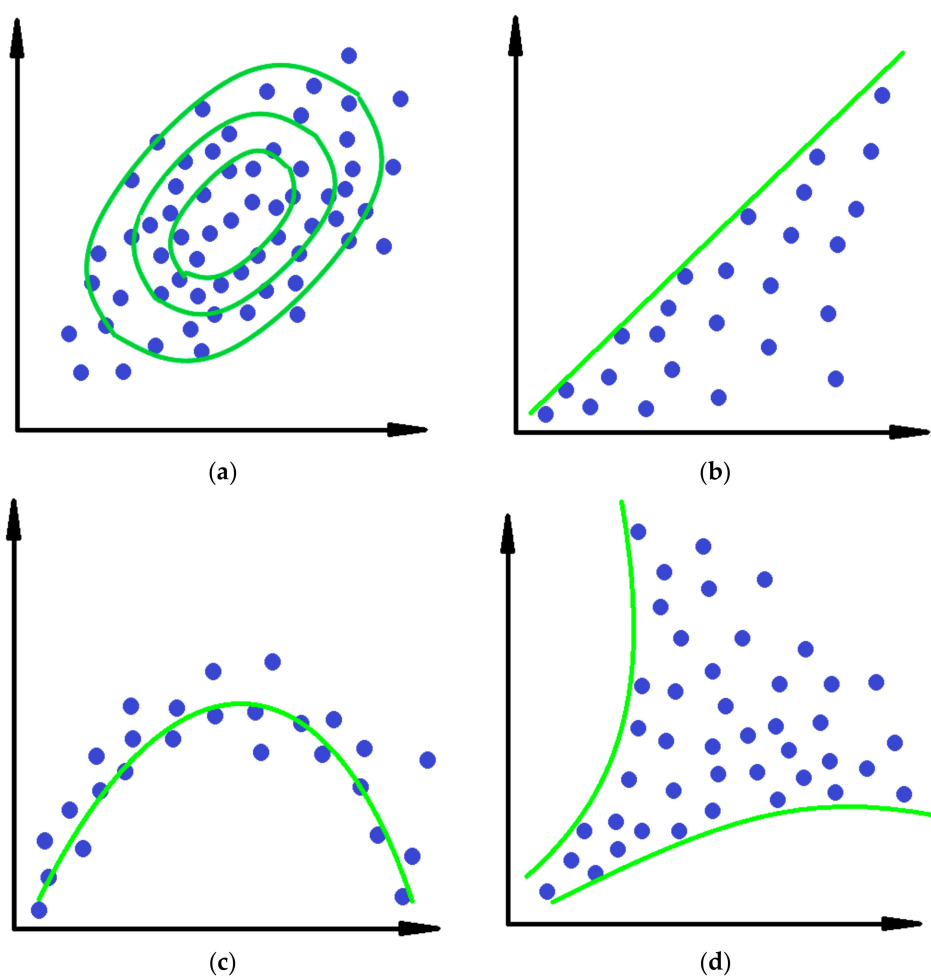


Figure 1. Schematic pattern of (a) multi-Gaussianity; multivariate complexities such as (b) constraint, (c) non-linearity and (d) heteroscedasticity.

2.2. Projection Pursuit Multivariate Transform Steps

The steps of projection pursuit multivariate transform are composed of preprocessing and projection pursuit. In the preprocessing steps, variables are transformed to normal score values and linear dependency is removed. In projection pursuit, complexity dependency is removed.

2.2.1. Preprocessing Steps

Normal Score Transformation

Consider data matrix A , which has M variables and N observations such that $A_{M \times N}$ is transformed through Equation (1) into normal score [29]:

$$A' = C^{-1}(E(A)) \quad (1)$$

where E and C^{-1} are original data cumulative distribution function (CDF) standard and normal data CDF, respectively.

Data Sphering

One of the requirements of the projection pursuit algorithm is to center the data with an orthogonal covariance matrix and variance, which can be done by applying the last preprocessing step, data sphering, which uses Equation (2):

$$P = R^{-\frac{1}{2}} B^T (A' - E\{A'\}) \quad (2)$$

where R and B are eigenvector and diagonal eigenvalue matrices, respectively, obtained from the A' covariance matrix's spectral decomposition.

Projection Pursuit

After completing the preprocessing steps, the projection pursuit algorithm can be computed, taking into consideration that projection is $Q = A\beta$, where β is the unit length vector of $h \times 1$ dimension related to projection Q . With multi-Gaussianity of A , every unit length vector β must yield a Q that is univariate Gaussian. In order to measure the univariate non-Gaussianity, the projection index $T(\beta)$ test statistic is designated; when projection Q is finely Gaussian, $T(\beta)$ is equal to zero. The projection pursuit algorithm uses optimized search, which is focused on identifying the β where the projection index $T(\beta)$ is the highest. Finding the highest projection index will also find the maximum non-Gaussian projection Q . Consequently, by using the determined optimum unit length vector β , data A is transformed to A'' , in which the projection is standard Gaussian, as $Q' = A''\beta$. In order to achieve this transformation, Equation (3) is used:

$$Z = [\beta, \gamma_1, \gamma_2, \dots, \gamma_{h-1}] \quad (3)$$

where values of γ are unit vectors obtained by applying the Gram–Schmidt algorithm to compute the orthogonal matrix of Z [32]. The next step is the transformation, which can be achieved by multiplying A and Z by each other (Equation (4)):

$$AZ = [Q, A\gamma_1, A\gamma_2, \dots, A\gamma_{h-1}] \quad (4)$$

The next step considers the X transformation, which yields the projection of standard Gaussian Q' while holding the same orthogonal matrix:

$$(AZ) = [Q', A\gamma_1, A\gamma_2, \dots, A\gamma_{h-1}] \quad (5)$$

The last step is multiplication of Z^T by $X(AZ)$, which results in back-transformation to the initial basis (Equation (6)):

$$A'' = X(AZ)Z^T \quad (6)$$

After back-transformation, optimized search can be used again to detect other complexities of A'' .

Stopping Criteria

To select the optimum value for projection index $T(\beta)$, considering the optimum h dimensions and number of N observations is critical due to the fact that a high value of h dimensions results in trouble with identifying the complexity, and a small amount of N observations leads to low reliability in detection. To choose the target projection index, a special algorithm is applied [22].

Application

Overall, the implementation of projection pursuit multivariate transformation on multivariate data is based on the forward- and backward-transformation techniques. For the sake of simplicity, Figure 2 shows a schematic illustration to explain the implementation of the PPMT technique [22].

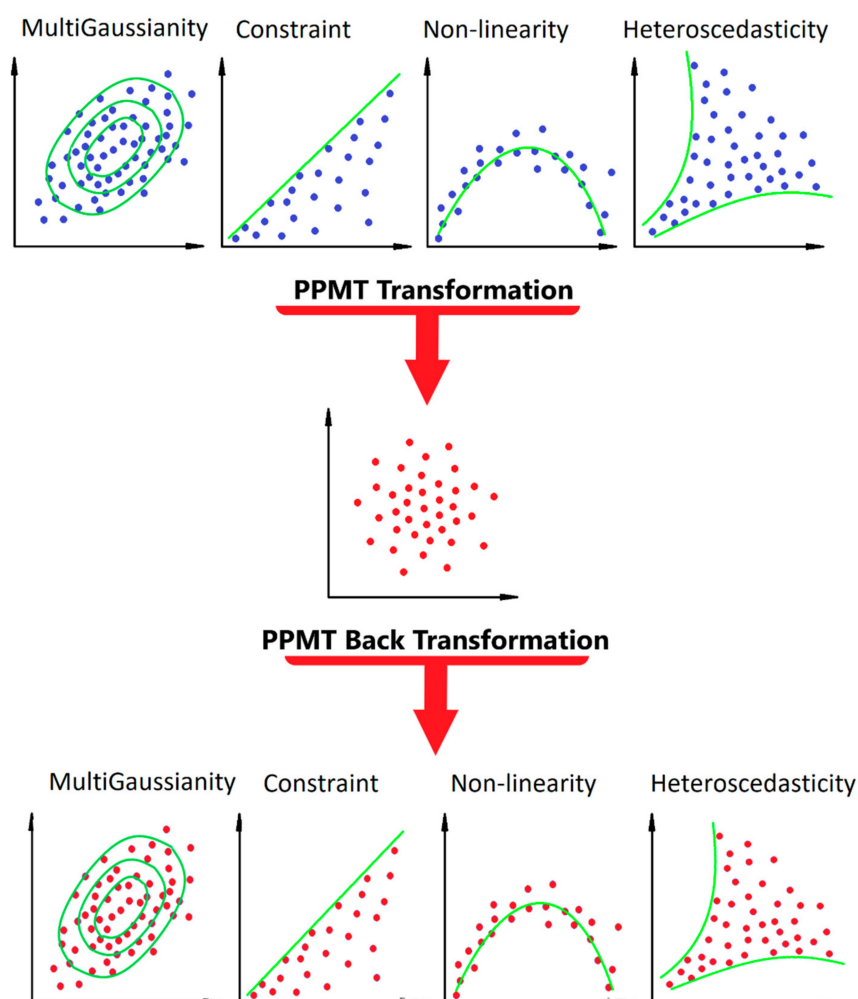


Figure 2. Representation of projection pursuit multivariate transformation (PPMT).

2.3. Proposed Algorithm

As already explained, the (co)-simulation approaches based on multi-Gaussianity assumptions (e.g., turning bands [33] and sequential Gaussian [34] co-simulation) are not suitable for modelling purposes with such bivariate complexity. On the contrary, PPMT is able to model these characteristics

based on factor transformation. In this technique, the dataset is first transferred to PPMT factors, in which the correlation among the factors become almost zero [22,24]. Since the cross-dependency among the factors is zero, the independent simulation can be applied over each factor and the outputs should be back-transformed to original scale. However, one of the main difficulties is related to the decorrelation step, where sometimes the forward transformation is not able to completely remove the inherent correlation between pairs of variables and a mild dependency may remain among the transformed factors that must not be negligible. One solution is to employ one more decorrelation steps, such as minimum/maximum autocorrelation factor (MAF) or principal component analysis (PCA), to make sure the correlation at lag 0 and other arbitrary lag is substantially removed. However, these methods do not guarantee that the correlation will be entirely eliminated through all other lags [35]. A way around this impediment is to co-simulate the PPMT factors even with small correlation that are left after forward transformation of the original variables to factors by inference of cross-dependency functions using the linear model of co-regionalization [25]. The output of the simulation is then back-transformed to original scale in the same way as in the independent simulation. In this paradigm, no MAF or PCA transformation is needed. The steps of the proposed algorithm are as follows:

1. Exploratory data analysis of multivariate data
2. Investigation of the level of complexity in bivariate relation analysis
3. PPMT forward transformation
4. Examination of removing cross-correlations among variables by using cross-correlogram
5. Inference of cross-dependency functions by linear model of co-regionalization (LMC)
6. (Co)-simulation of PPMT transformed factors taking into account the fitted LMC
7. PPMT backward transformation of simulated results (realizations) into original scale
8. Validation of the output by statistical analysis tools

In order to show the capability of the proposed model, a case study is presented and the outputs after validation are taken into account for mineral resource classification, a critical issue in international reporting of deposits.

3. Case Study: Aktas-South Deposit in Kazakhstan

This case study is the Aktas-South deposit, which is located in Reddipalayalam, in the state of Tamil Nadu, south of Kazakhstan. The deposit is limestone being used at a cement plant that belongs to the Aktas Group. For confidentiality reasons, the exact location of the deposit is not disclosed. The regional geology of this deposit falls in the Masanchi and Uzun formations in the group of Sabanbay rocks. The limestone in the deposit refers to Masanchi formation. The whole sedimentary formation of this zone is related to marine origin due to marine transgressions and regressions with corresponding fluctuations. As the limestone beds lack marl intrusions, they are composed of clusters of marine organisms. The limestone in the Aktas South area is divided into four groups according to their outward aspects, as shown in Table 1.

Table 1. Division of limestone in Aktas South region.

Lithology	Physical Appearance	Chemical Characteristics	Comment
Cherty limestone (CL)	Yellow in color with alternating cherty bands	Not ascertained	Likely to be used in cement after removing cherty bands
Pale yellow limestone (PYLS)	Yellow to pale brown in color	>40% CaO and <3.5% Fe ₂ O ₃	Very good for cement manufacturing
Brown cherty limestone (BCLS)	Brown to dark brown	>8% Fe ₂ O ₃	
Ferruginous limestone (FLS)	Brown to dark brown	>40% CaO and Fe ₂ O ₃ > 3.5% to 10	Considered as low grade limestone

3.1. Exploratory Data Analysis in Limestone Deposit

The dataset consists of 4553 samples with homotopic sampling patterns. This configuration means that the data are available through all sample points and all variables have been assayed on equal sets of sample locations [36].

The dataset is composed of four chemical compounds: iron oxide (Fe_2O_3), aluminum oxide (Al_2O_3), silicon oxide (SiO_2), and calcium oxide (CaO), whose values are assayed in percentages. Similar to all geostatistical projects, the first step is exploratory data analysis to identify global statistical characteristics of the underlying variables. First, possible outliers and duplicated data were recognized. The presence of outliers in the dataset makes the inference of statistical parameters problematic and nonrepresentative [37,38]. These aberrant values intentionally influence the variance and result in sharp fluctuations in variogram analysis [39]. In addition, detection and removal of duplicate data is also important prior to any geostatistical analysis. One of the problems is that these repeated values generate singular matrices in kriging systems, leading to unestimated blocks surrounding the duplicate locations [40]. After removing duplicate locations in this study, the variables are plotted in a probability plot. This statistical tool helps to detect and fix extreme and innermost values [41]. Following this, some outlier values are detected for Fe_2O_3 and CaO (Figure 3). In the distribution of Fe_2O_3 , values more than about 18% are considered as extreme values, and in the distribution of CaO , values less than about 19% are recognized as innermost values, while the other two distributions (SiO_2 and Al_2O_3) sound reasonable given that no significant outliers were identified.

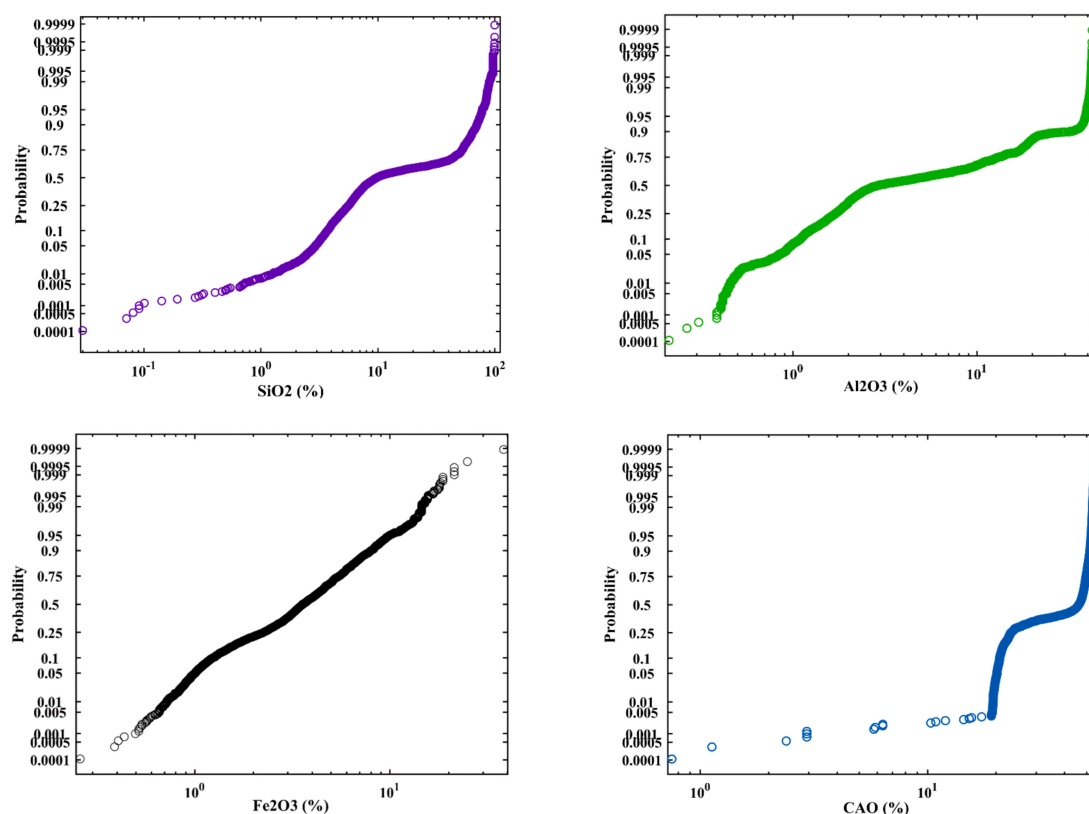


Figure 3. Probability plots of chemical compounds that identify extreme and innermost values.

Once these outlier values are detected, the capping approach [41] is applied to treat them accordingly in order to preserve them in the dataset after examining whether they are valid samples and not erroneous. In this technique, the values in the upper and lower tails of the distribution should be moved back to the previous maximum value and forward to the next minimum value, respectively.

The next step in statistical analysis is related to the declustering process. This step was not necessary, as the sampling pattern is almost regular in the region (Figure 4). The most critical chemical compounds for this deposit are related to the variability of CaO and SiO₂. These two variables introduce high-quality limestone for high amounts of CaO (>10%) and low amounts of SiO₂ (<40%). In addition, Fe₂O₃ plays an important role, yet does not have as significant an influence as SiO₂ in favor of CaO. As can be seen, the majority of drillholes illustrate a high concentration of CaO, which is distributed homogeneously in the region. Interestingly, SiO₂ reveals poor concentration in the same locations, meaning it satisfies the quality of limestone for the entire deposit, corroborating high CaO and low SiO₂. This visual inspection also indicates a strong spatial dependency between CaO and SiO₂, in which there is a negative impact on the local distribution of these two chemical compounds. This shows a high concentration of CaO versus a low concentration of SiO₂, which is important for this deposit. This phenomenon motivates a further investigation into the cross-correlation structures among these chemical variables toward better decision making for the selection of efficient geostatistical algorithms for 3D modelling and mineral resource evaluation.

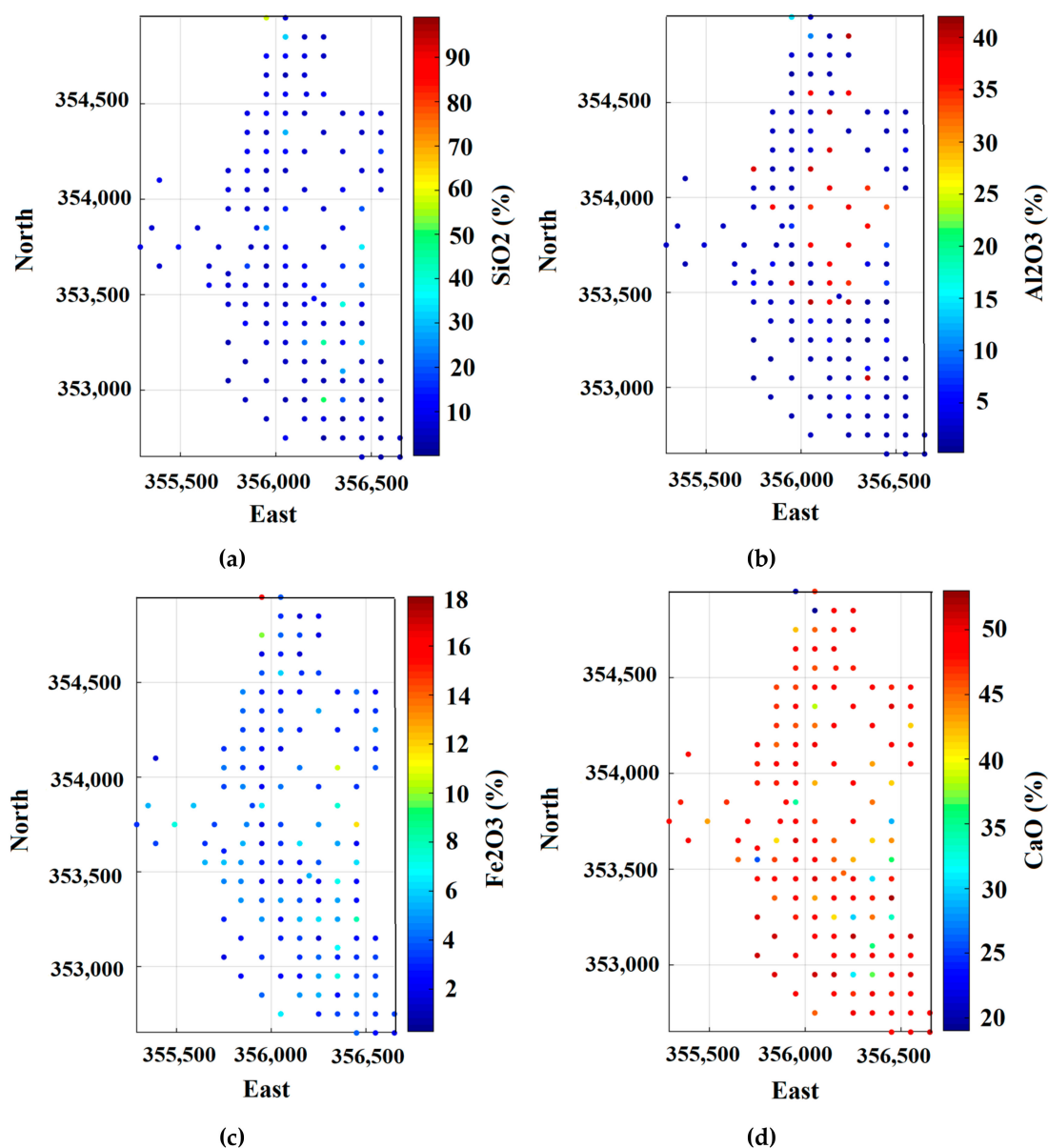


Figure 4. Location map of drilling patterns in limestone deposit.

Then, statistical parameters of the data were computed, as shown in Table 2. The coefficient of variation (COV) for all variables, particularly CaO and SiO₂, is less than 2.0, which indicates that the distribution of data has no significant harsh variability and predictive models can be suitable and meaningful [41]. In this limestone deposit, as previously mentioned, CaO and SiO₂ are two critical variables for ore/waste selection. For this purpose, areas with more than 10% CaO and less than 40% SiO₂ define ore zones, and areas with less than 10% CaO and more than 40% SiO₂ introduce waste zones based on mining excavation destination. Before initiating the modelling process, it might be of interest to calculate two global recovery functions, fraction of recoverable ore above or below the cutoff and mean grade above or below the cutoff [28,42]. These two parameters are calculated by bivariate cumulative distribution functions computed over CaO and SiO₂ as follows:

Fraction of total tonnage in the specified cutoff for ore:

$$T(\text{CaO} > 10\% \mid \text{SiO}_2 \leq 40\%) = 66.20\%$$

Mean grade in the specified cutoff for CaO in ore:

$$m(\text{CaO} > 10\% \mid \text{SiO}_2 \leq 40\%) = 9.19\%$$

These two parameters show that about 66.2% and 33.8% of the entire deposit may be ore and waste, respectively, which is an interesting economical characteristic of this mine deposit.

Table 2. Statistical univariate parameters of original Al₂O₃, CaO, Fe₂O₃, and SiO₂ in the dataset of Aktas-South deposit.

Variable (%)	Number of Samples	Minimum	Maximum	Mean	Variance	Coefficient of Variation (COV)
Al ₂ O ₃	4553	0.21	42.32	9.33	132.92	1.23
CaO	4553	0.75	53.94	38.79	164.14	0.33
Fe ₂ O ₃	4553	0.26	38.24	4.29	9.04	0.70
SiO ₂	4553	0.03	99.37	27.24	744.72	1.00

In order to investigate the cross-dependency among these four chemical compounds, the global correlation coefficient was calculated, as presented in Table 3. Fairly good negative and positive correlations can be seen between Fe₂O₃ and CaO (−0.64) and between Fe₂O₃ and SiO₂ (approximately 0.53). The highest dependency is seen between CaO and SiO₂, which has negative correlation with almost −0.94 correlation coefficient. This corroborates the visual interpretation already provided in the location map of sampling points (Figure 4). Other correlations, such as those between Fe₂O₃ and Al₂O₃, Al₂O₃ and CaO, and Al₂O₃ and SiO₂, are somewhat low. These values only give a general perspective on the linear dependency that exists among the variables and may not be suitable for examining whether or not complex characteristics such as nonlinearity, heteroscedasticity, and geological constraints may exist. In order to examine the latter characteristics, the bivariate relation in Figure 5 is presented as scatter plot between pairs of the variables Al₂O₃, CaO, Fe₂O₃, and SiO₂. This statistical diagram is suitable to explore relationships such as complexities and linearity features between pairs of variables. This is an interesting illustration of different complexities between co-variables, starting from heteroscedastic characteristics between Fe₂O₃ and Al₂O₃, and CaO and SiO₂; nonlinearity observed between SiO₂ and CaO; and geologic constraints between CaO and Al₂O₃.

Table 3. Correlation coefficients between pairs of variables in Aktas-South limestone deposit.

Variables	Fe ₂ O ₃	Al ₂ O ₃	CaO	SiO ₂
Fe ₂ O ₃	1	0.13	−0.64	0.53
Al ₂ O ₃		1	−0.17	0.13
CaO			1	−0.94
SiO ₂				1

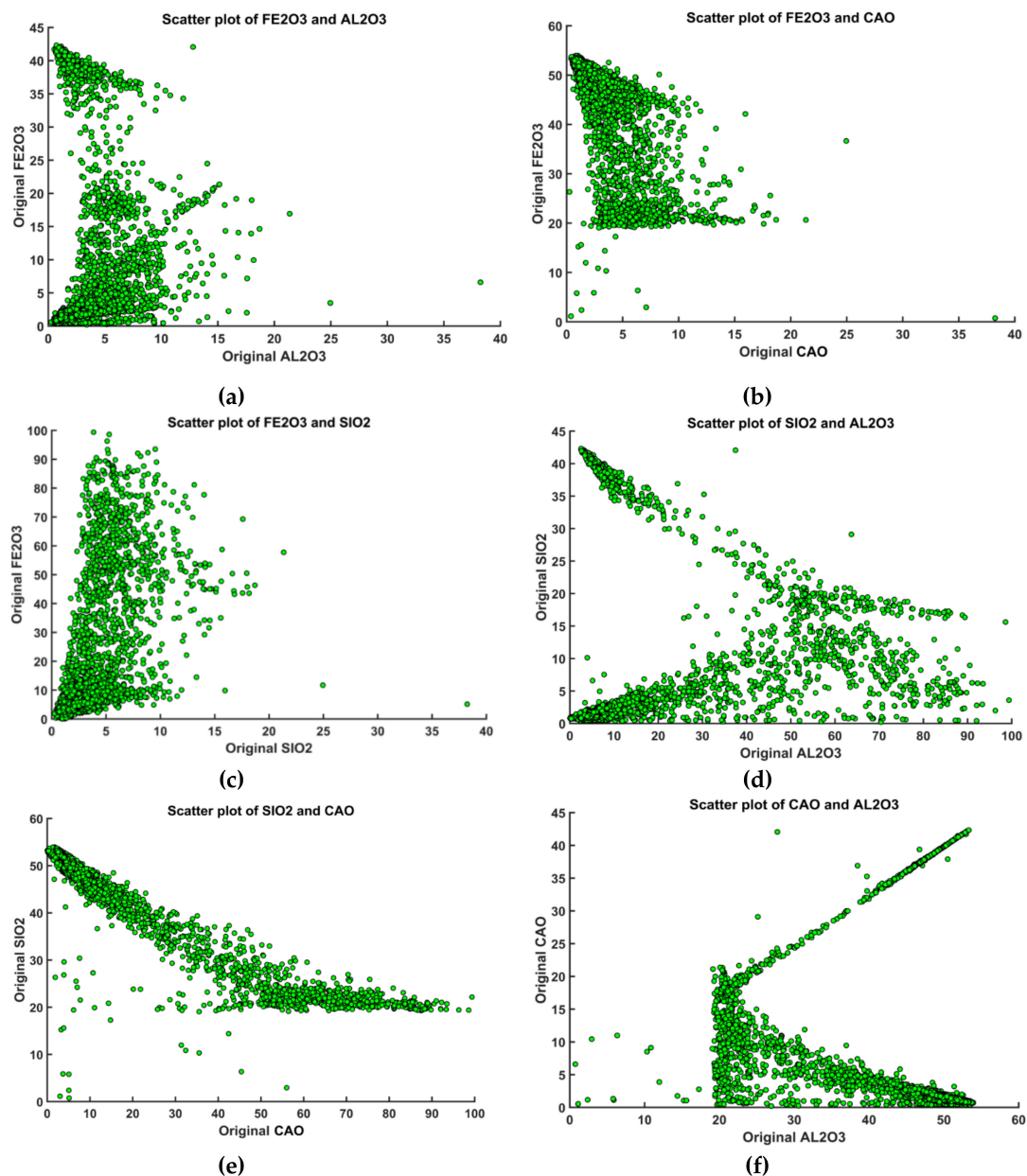


Figure 5. Scatter plots of (a) Fe_2O_3 and Al_2O_3 , (b) Fe_2O_3 and CaO , (c) Fe_2O_3 and SiO_2 , (d) SiO_2 and Al_2O_3 , (e) SiO_2 and CaO , (f) CaO and Al_2O_3 .

3.2. PPMT Forward Transformation

As mentioned before, one of the objectives of this paper is to jointly model variables by considering original correlations among variables to reconstruct the shape of complex bivariate relations. It is explained that correlation shapes between pairs of variables are complex (Figure 5). These types of features motivate the use of factorization approaches such as projection pursuit multivariate transform (PPMT) to jointly model the underlying four variables (Al_2O_3 , CaO , Fe_2O_3 , and SiO_2). The result of this modelling approach is then applied for mineral resource classification. However, prior to any geostatistical modelling, whether it is independent simulation or co-simulation after forward PPMT transformation, the removal of correlations after this first transformation should be assessed. Therefore, in this study, as a common practice in forward PPMT transformation, the variables are first transformed to PPMT factors and then undergo one further transformation by MAF, implemented to completely remove cross-correlation. This can be evaluated by a cross-correlogram (Figure 6).

The results of the cross-correlogram between MAF factors show that a small amount of correlation is still resistant in some lags. For instance, one can recognize that the correlation in the first lag (~100 m) is around 25% between SiO_2 and Al_2O_3 even after this MAF transformation (Figure 6). This signifies that MAF is not able to decorrelate the variables over all the lag separations. In this respect, it is not advocated to use the independent simulation due to the remaining small correlations among factors. In order to cope with the proposed algorithm in this case, it was decided to employ co-simulation right after the initial PPMT forward transformation of underlying variables irrespective of considering any further MAF transformation. For this, once again, the cross-correlation among the transformed PPMT factors is examined through the cross-correlogram and before the MAF step. The results show that the correlation manifests itself through some lags (e.g., ~12% between SiO_2 and CaO at a lag separation of 150 m and ~11% between SiO_2 and Al_2O_3 at a lag separation of 400 m; Figure 7), although at a lag separation of 0, the correlation is significantly removed (Figure 8). Even these small amounts of correlation among the PPMT factors are important and provoke applying the co-simulation algorithms via PPMT transformed factors and considering the linear model of co-regionalization.

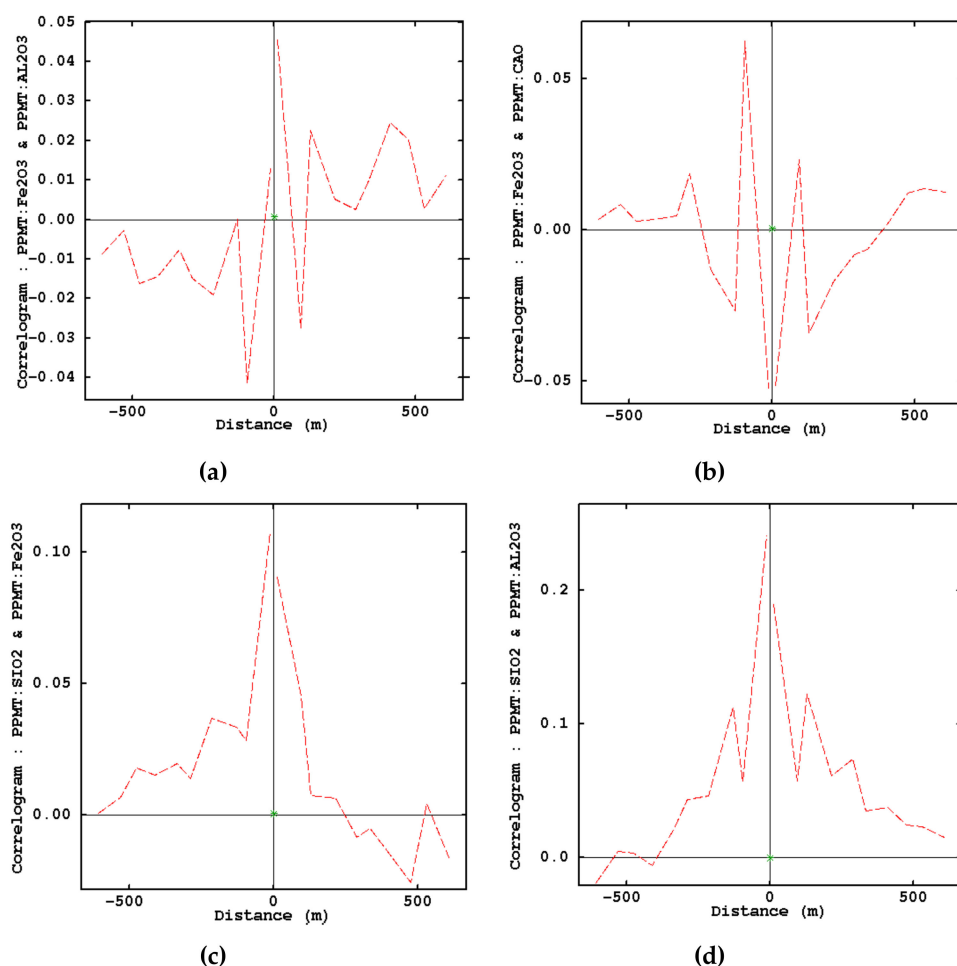


Figure 6. *Cont.*

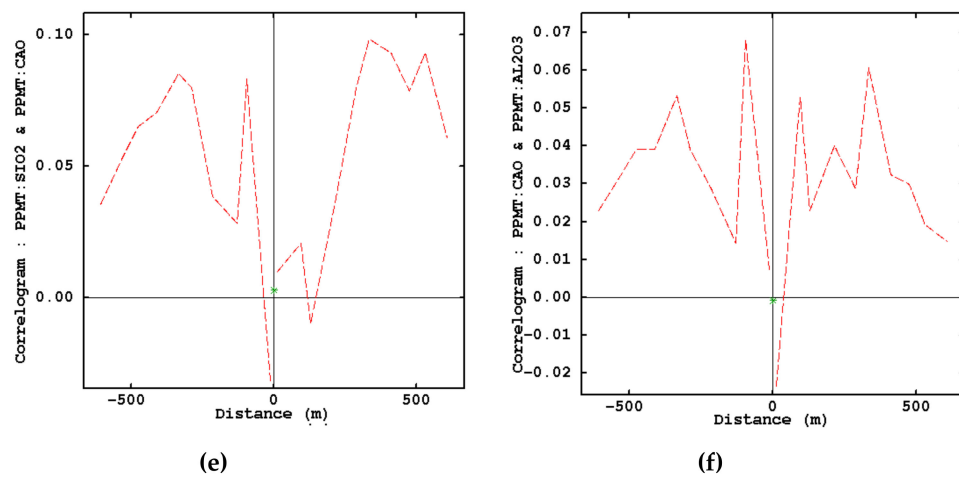


Figure 6. Correlograms of PPMT factors with minimum/maximum autocorrelation factor (MAF) transformation ((a) PPMT Fe₂O₃ and PPMT Al₂O₃, (b) PPMT Fe₂O₃ and PPMT CaO, (c) PPMT SiO₂ and PPMT Fe₂O₃, (d) PPMT SiO₂ and PPMT Al₂O₃, (e) PPMT SiO₂ and (f) PPMT CaO, PPMT CaO and PPMT Al₂O₃).

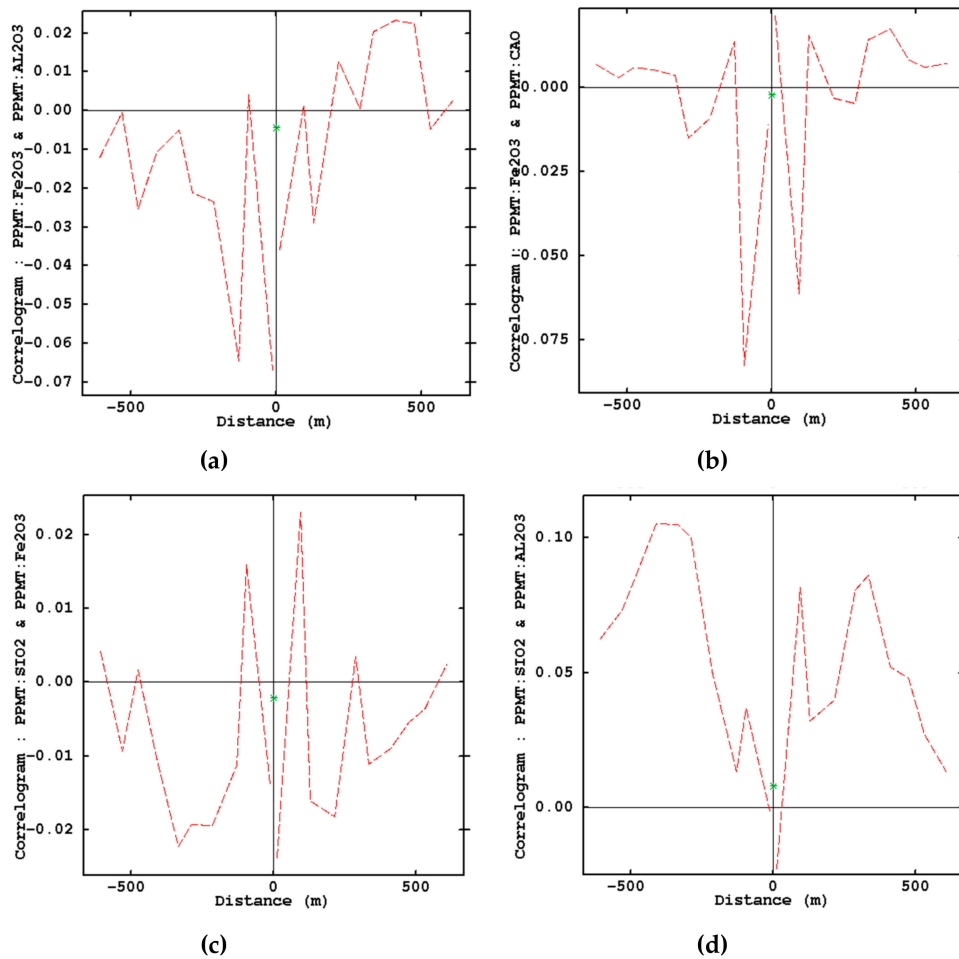
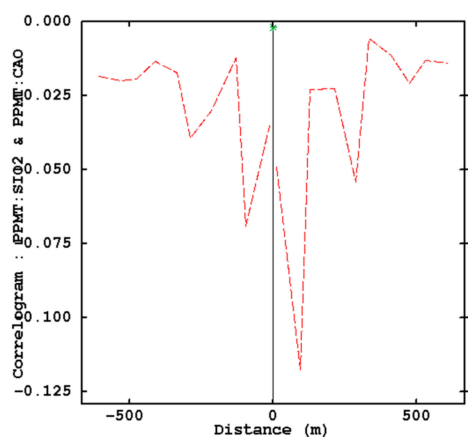
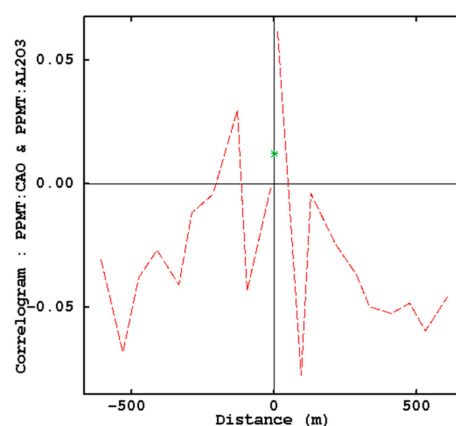


Figure 7. *Cont.*

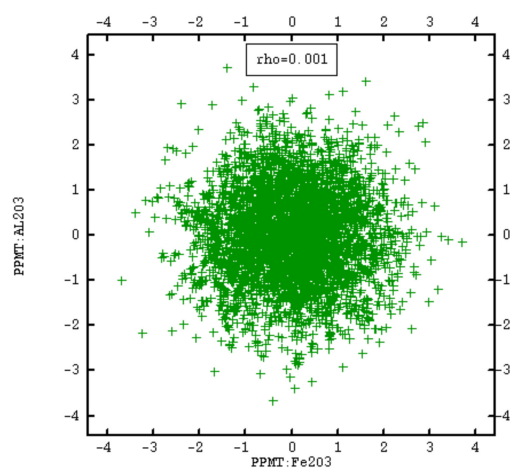


(e)

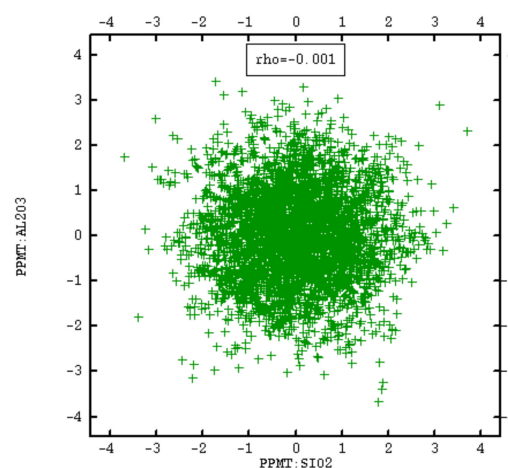


(f)

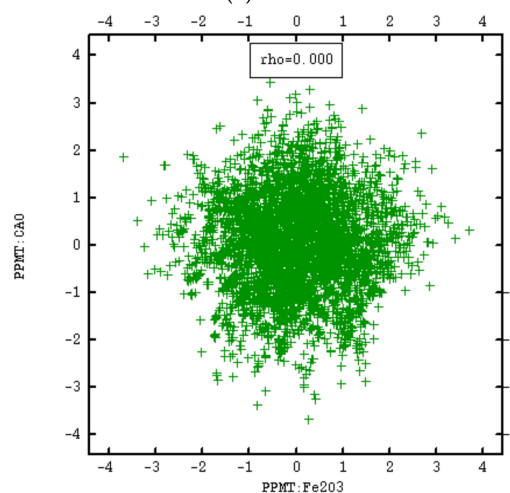
Figure 7. Correlograms of PPMT factors without MAF transformation ((a) PPMT Fe₂O₃ and PPMT Al₂O₃, (b) PPMT Fe₂O₃ and PPMT CaO, (c) PPMT SiO₂ and PPMT Fe₂O₃, (d) PPMT SiO₂ and PPMT Al₂O₃, (e) PPMT SiO₂ and PPMT CaO, (f) PPMT CaO and PPMT Al₂O₃).



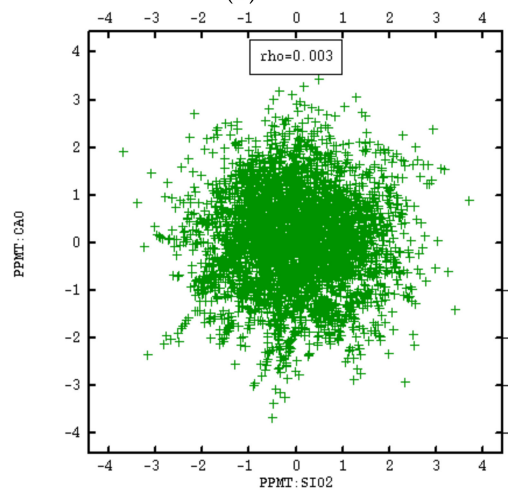
(a)



(b)



(c)



(d)

Figure 8. Cont.

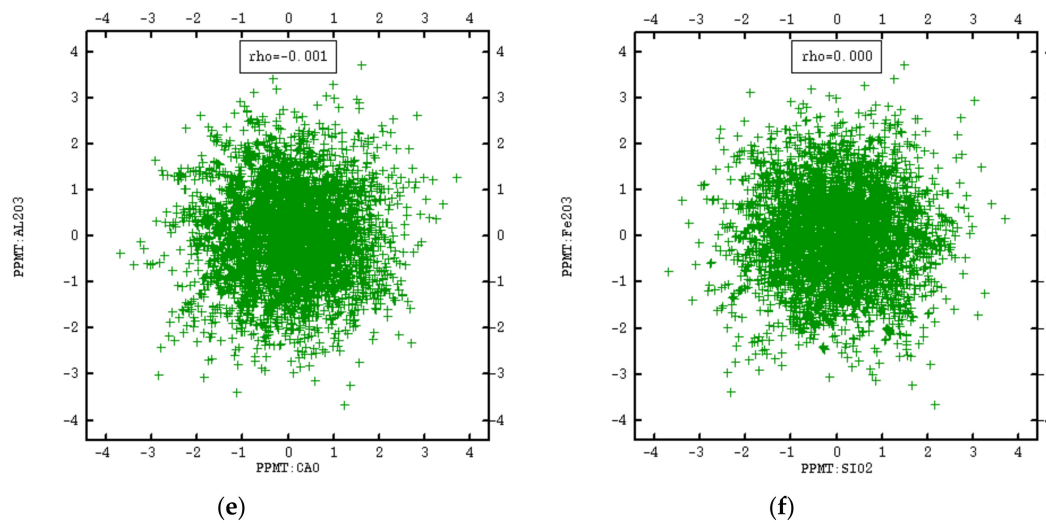


Figure 8. Scatter plots of transformed variables without integration of MAF: (a) PPMT_Al₂O₃ and PPMT_Fe₂O₃, (b) PPMT_Al₂O₃ and PPMT_SiO₂, (c) PPMT_CaO and PPMT_Fe₂O₃, (d) PPMT_CaO and PPMT_SiO₂, (e) PPMT_Al₂O₃ and PPMT_CaO, (f) PPMT_Fe₂O₃ and PPMT_SiO₂. Correlation at lag 0 is almost zero.

3.3. Variogram Inference

As mentioned in a previous section, the transformed factors retain the correlation at other lag distances except zero, and a further decorrelation transformation technique such as MAF cannot completely remove the inherent correlations. Following the proposed algorithm in this research, the next step is variogram analysis over the transformed variables. This step is needed to establish the co-kriging system in co-simulation algorithms, taking into account the linear model of co-regionalization. This latter introduces even small correlations in co-simulation algorithms. In this respect, inference of direct and cross-variograms for all four PPMT transformed variables is implemented. The sill of experimental cross-variogram as a measure of joint variability to some extent reflects the magnitude of the correlation between the variables [43]. In the case of standardized variables (variance equal to 1), the sill of cross-variograms must be the cross-correlation between collocated values of those variables [44].

It is also worth mentioning that anisotropy was examined through the original dataset (not transformed), and it was seen that the existence of anisotropy in the region was improbable. For fitting of theoretical variograms over experimental variograms, the linear model of co-regionalization [45] with semi-automatic technique is chosen, in which the semi-definiteness condition [36,46] is respected through the process of fitting. In this model, direct and cross-covariances are defined as the sum of basic covariances. Therefore, by this technique and after computation of experimental variograms, two nested structures (spherical, with the first scale factor as 54 m and the second scale factor as 216 m) are fitted accordingly, with no nugget effect, as can be seen in Figure 9 (Equation (7)).

$$\begin{pmatrix}
 Y_{Al_2O_3} & Y_{CaO/Al_2O_3} & Y_{Fe_2O_3/Al_2O_3} & Y_{SiO_2/Al_2O_3} \\
 Y_{CaO/Al_2O_3} & Y_{CaO} & Y_{Fe_2O_3/CaO} & Y_{SiO_3/CaO} \\
 Y_{Fe_2O_3/Al_2O_3} & Y_{Fe_2O_3/CaO} & Y_{Fe_2O_3} & Y_{SiO_2/Fe_2O_3} \\
 Y_{SiO_2/Al_2O_3} & Y_{SiO_2/CaO} & Y_{SiO_2/Fe_2O_3} & Y_{SiO_2}
 \end{pmatrix}
 = \begin{pmatrix}
 0.499 & 0.060 & -0.002 & 0.003 \\
 0.006 & 0.499 & -0.001 & -0.001 \\
 -0.002 & -0.001 & 0.499 & -0.001 \\
 0.003 & -0.001 & -0.001 & 0.499
 \end{pmatrix} \text{spherical (54 m, 54 m, 54 m)} \quad (7)$$

$$+ \begin{pmatrix}
 0.499 & 0.060 & -0.002 & 0.003 \\
 0.006 & 0.499 & -0.001 & -0.001 \\
 -0.002 & -0.001 & 0.499 & -0.001 \\
 0.003 & -0.001 & -0.001 & 0.499
 \end{pmatrix} \text{spherical (216 m, 216 m, 216 m)}$$

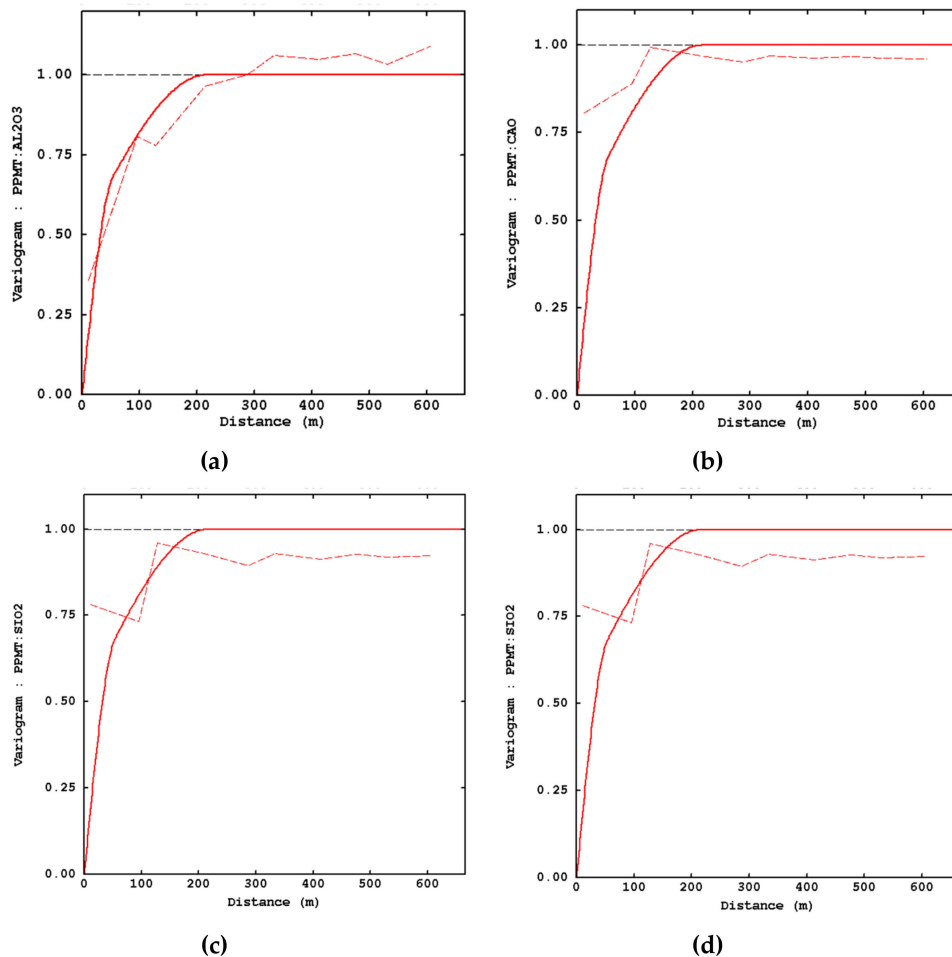


Figure 9. Fitted direct variograms of transformed variables: (a) PPMT Al_2O_3 , (b) PPMT CaO, (c) PPMT SiO_2 , (d) PPMT SiO_2 . For brevity, only direct variograms are presented.

3.4. Stochastic Modeling in Limestone Deposit

After variogram inference over PPMT transformed covariates and following the proposed algorithm in this study, the step for implementing co-simulation takes into account grid nodes with dimensions of $48\text{ m} \times 48\text{ m} \times 11\text{ m}$ for each block to jointly model all transformed factors. Turning bands co-simulation (TBCOSIM) is selected because of its versatility and reliability in reproducing global and statistical parameters when compared to other Gaussian co-simulation algorithms [47]. In this method,

each variable is first simulated nonconditionally and then through a post-processing step by co-kriging conditioned on the available information and borehole records [33]. In this regard, ordinary co-kriging is used with moving neighborhood ranges equal to the range of variograms (200 m) attending up to 50 nearest surrounding sample points in the process of conditioning. Multiple-search strategy is also selected for this purpose, since it shows better results compared to single-search strategy [48]. One of the main criticisms against TBCOSIM, however, is related to producing artifacts because of turning lines. To deal with this difficulty, the number of lines should be reasonably increased [33,49]. Therefore, 1000 lines was set for the turning bands simulation method to eliminate possible stripping effects. The number of realizations was considered to be 100. The realizations that interpret the spatial variability of each factor were then back-transferred to original scale through backward PPMT transformation. Next, E-type maps were generated by averaging through 100 realizations within each block in co-simulated element over the variability in original scale. E-type maps of CaO, Al₂O₃, Fe₂O₃, and SiO₂ were produced through 100 realizations, as shown in Figure 10. Before further analysis over the simulated results, it is necessary to check whether the outputs of this proposed algorithm are statistically valid.

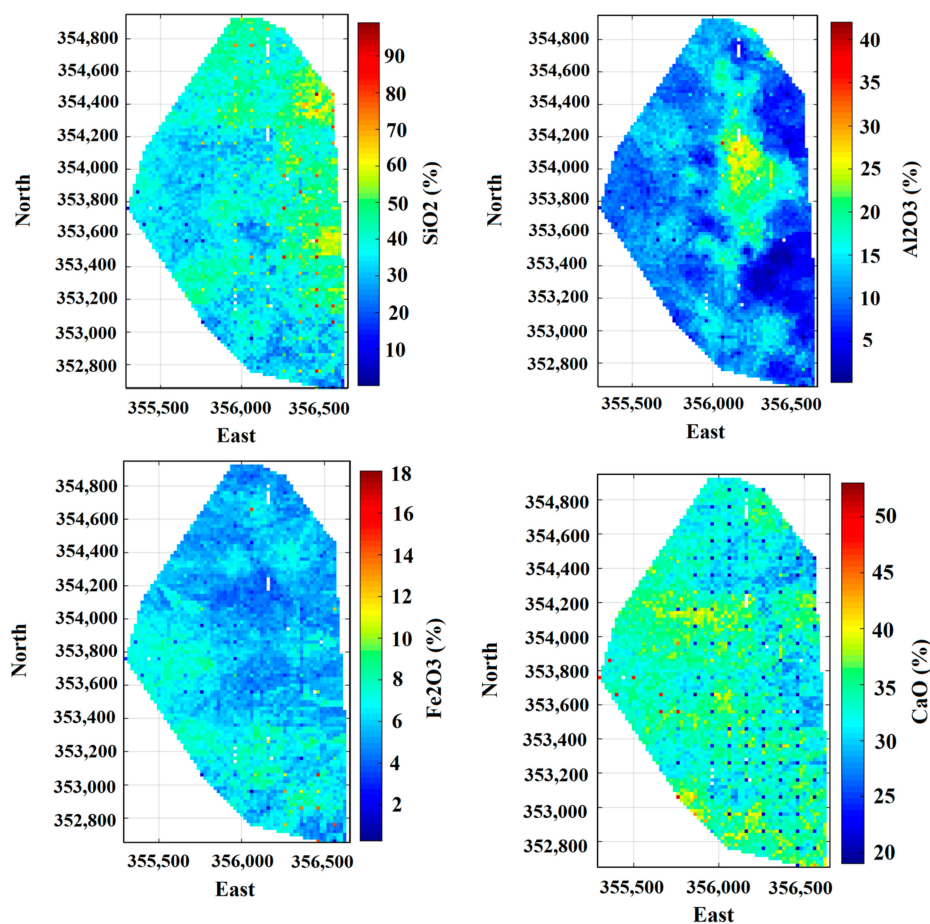


Figure 10. E-type maps of all underlying elements according to PPMT methodology.

3.5. Validation

Validation analysis in this section is concerned with the reproduction of original statistical characteristics such as mean, variance, correlation coefficient, and shape of bivariate relation. This type of validation process is required to give practitioners insight with regard to the level of reliability of the aforementioned approach in the section on mineral resource estimation and classification. A comparison between the means of original variables (Fe₂O₃, Al₂O₃, SiO₂, and CaO) and the means

of simulated and back-transformed variables calculated from PPMT through 100 realizations is shown in Figure 11. As can be seen, PPMT is able to reproduce the original mean values of each variable.

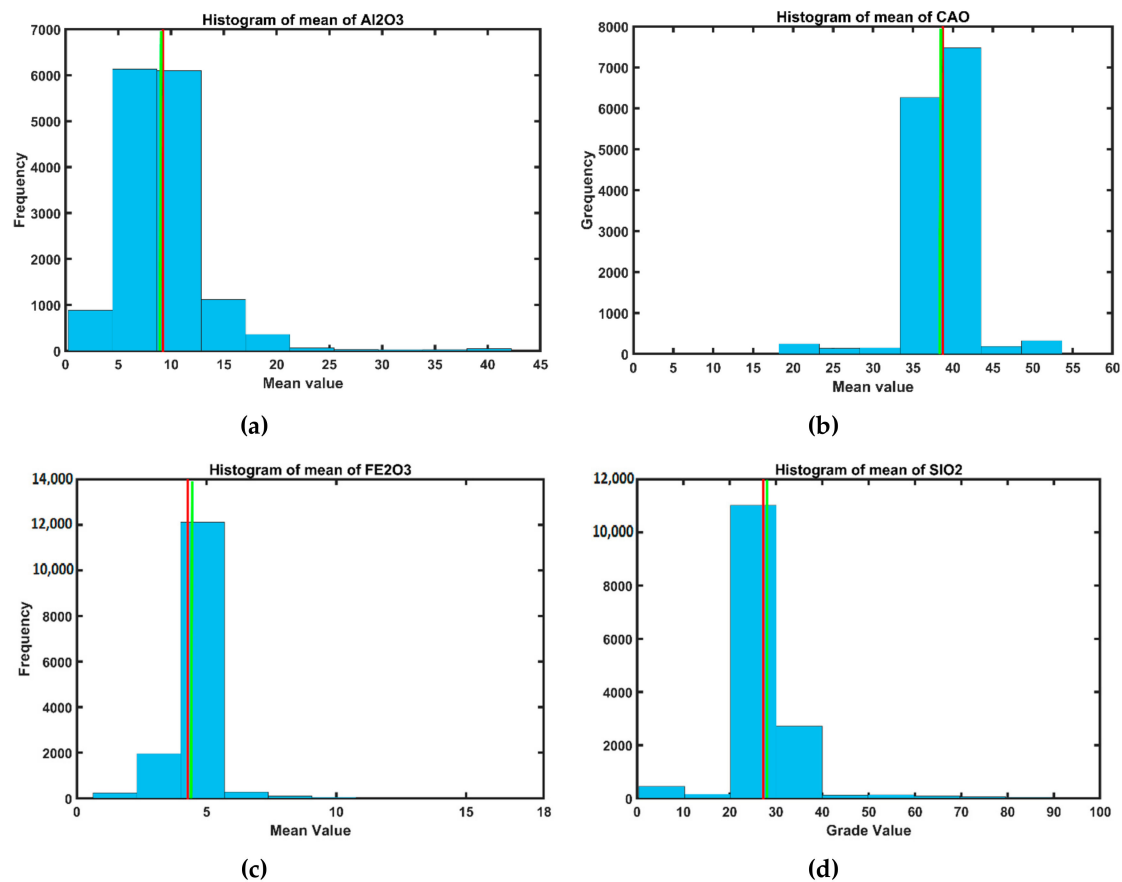


Figure 11. Histograms of mean values of: (a) aluminium oxide (Al_2O_3), (b) calcium oxide (CaO), (c) iron oxide (Fe_2O_3) and (d) silicon oxide (SiO_2) obtained from PPMT method. Green line is the average of mean values over 100 realizations; red line represents the original mean of variables.

The next comparison is the reproduction of global statistical analysis between variance of original variables (Fe_2O_3 , Al_2O_3 , SiO_2 , and CaO) and simulated and back-transformed values obtained from the PPMT method through 100 realizations. For CaO and SiO_2 (Figure 12), it is intuitively determined that PPMT produces satisfactory outputs in terms of reproduction of variance. However, minor deviations, such as for Fe_2O_3 , as can be seen from this figure, are referred to the influence of conditioning data [24,50,51]. However, this tiny departure of average of variances for 100 realizations from original variance is not remarkably significant.

Finally, yet importantly, comparisons of correlation coefficients provided by PPMT and original correlation coefficients are examined among all variables (Fe_2O_3 , Al_2O_3 , SiO_2 , and CaO) through 100 realizations. As it can be seen from Figure 13, co-simulation methodology shows satisfactory results in the reproduction of original correlation coefficients among co-variables. This good performance among variables can be explained by the fact that co-simulation considers the intrinsic correlation between variables by incorporating the linear model of co-regionalization [51–53].

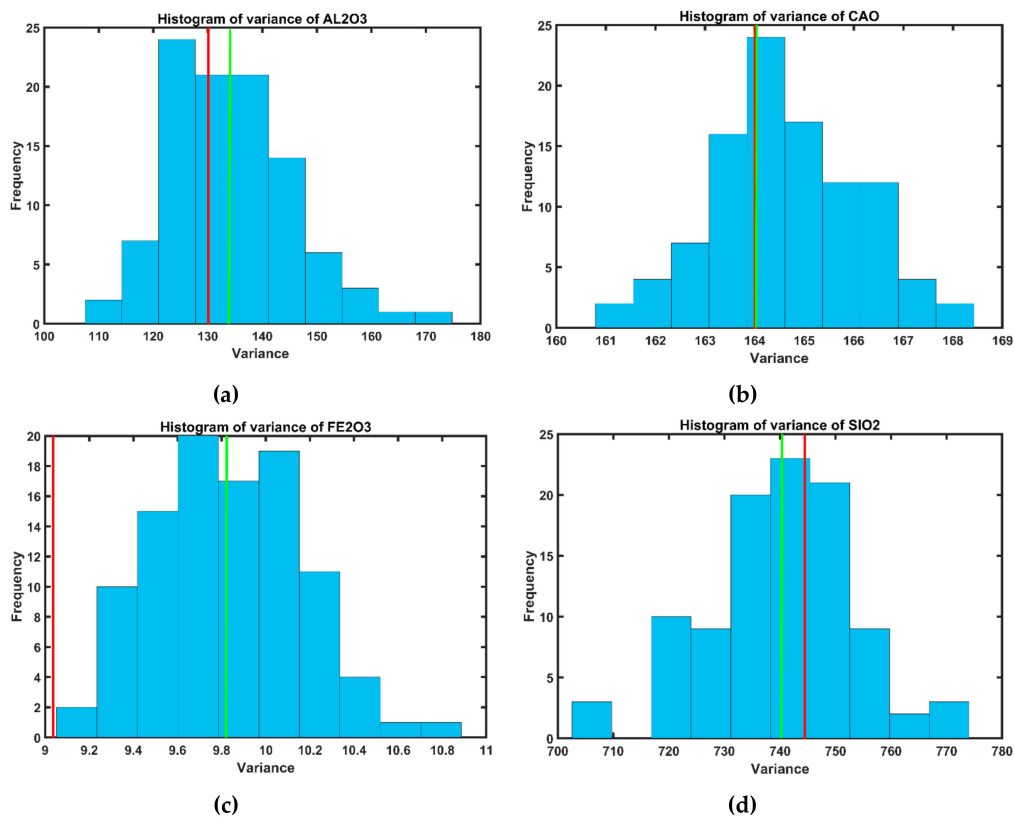


Figure 12. Histograms of mean variance of: (a) aluminium oxide (Al₂O₃), (b) calcium oxide (CaO), (c) iron oxide (Fe₂O₃), and (d) silicon oxide (SiO₂) obtained from PPMT method. Green line is the average mean of 100 realizations; red line represents the original mean of variables.

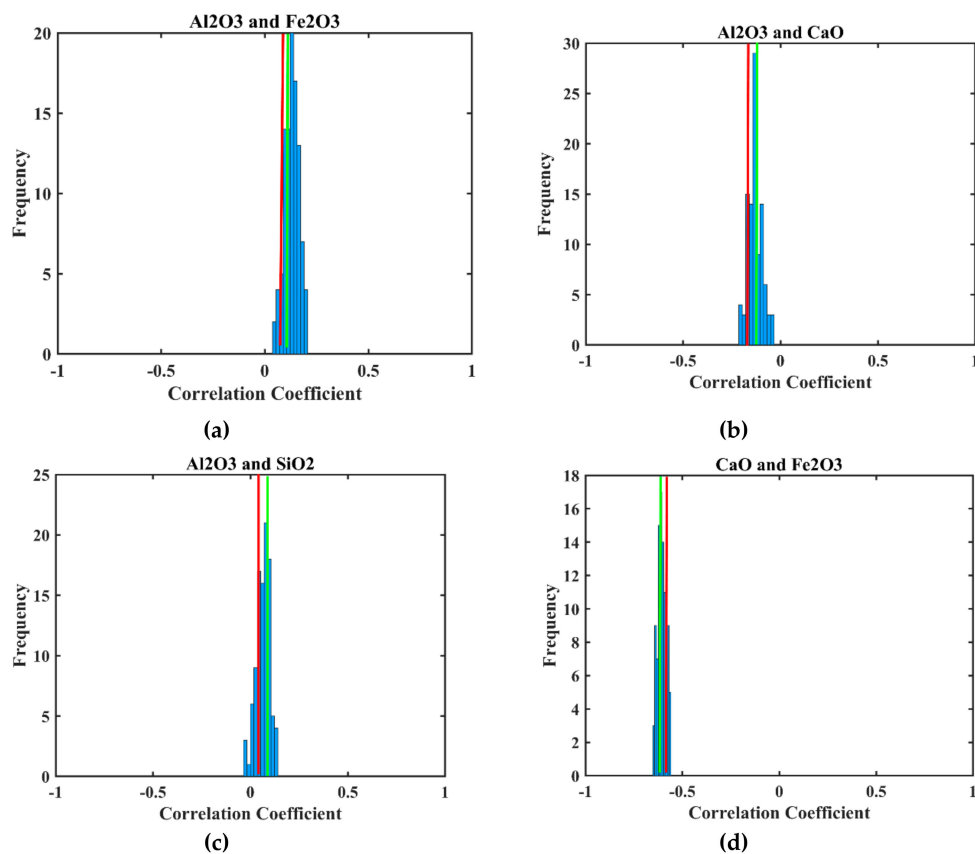


Figure 13. Cont.

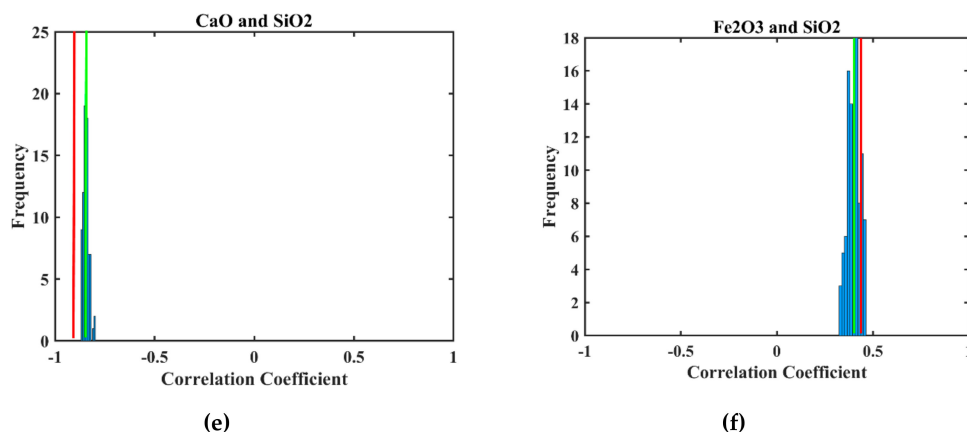


Figure 13. Graphs of correlation coefficients of: (a) Al_2O_3 and Fe_2O_3 , (b) Al_2O_3 and CaO , (c) Al_2O_3 and SiO_2 , (d) CaO and Fe_2O_3 , (e) CaO and SiO_2 , (f) and Fe_2O_3 and SiO_2 obtained by PPMT method. Green line is the average mean of 100 realizations; red line represents the original correlation coefficient between variables.

Another part of the comparison is related to examining the ability of the proposed method to reconstitute the shape of the original bivariate relations between pairs of chemical compounds. By visual inspection of reproductions of the shape of correlation for the underlying pairs of variables, one can see the difference between original and reproduced shapes in Figure 14. It should be mentioned that only one realization was taken to illustrate the reproduction of correlation shape, and it was randomly chosen as a first realization for all cases for the sake of fairness. As can be seen from the scatter plots of Fe_2O_3 and Al_2O_3 , PPMT co-simulation successfully reproduces the shape of original correlation. The same features are evidently demonstrated in the reproduction of the shape of original correlation between Fe_2O_3 and CaO , Fe_2O_3 and SiO_2 , and SiO_2 and CaO . However, inadequate results in the reproduction of the shape of correlation between SiO_2 and Al_2O_3 , and CaO and Al_2O_3 can be seen. Overall, the proposed approach based on the combination of PPMT and co-simulation is capable of reconstructing the original shape of correlation.

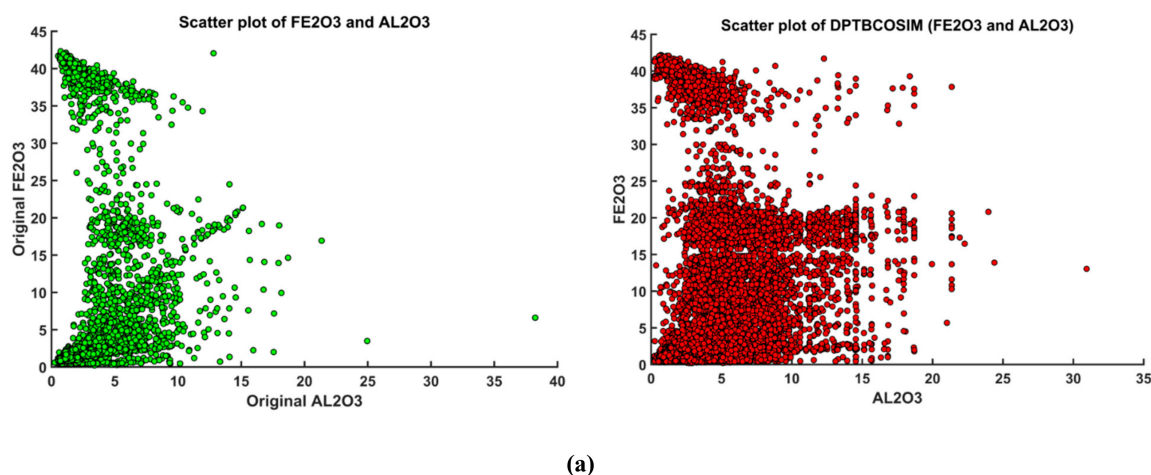
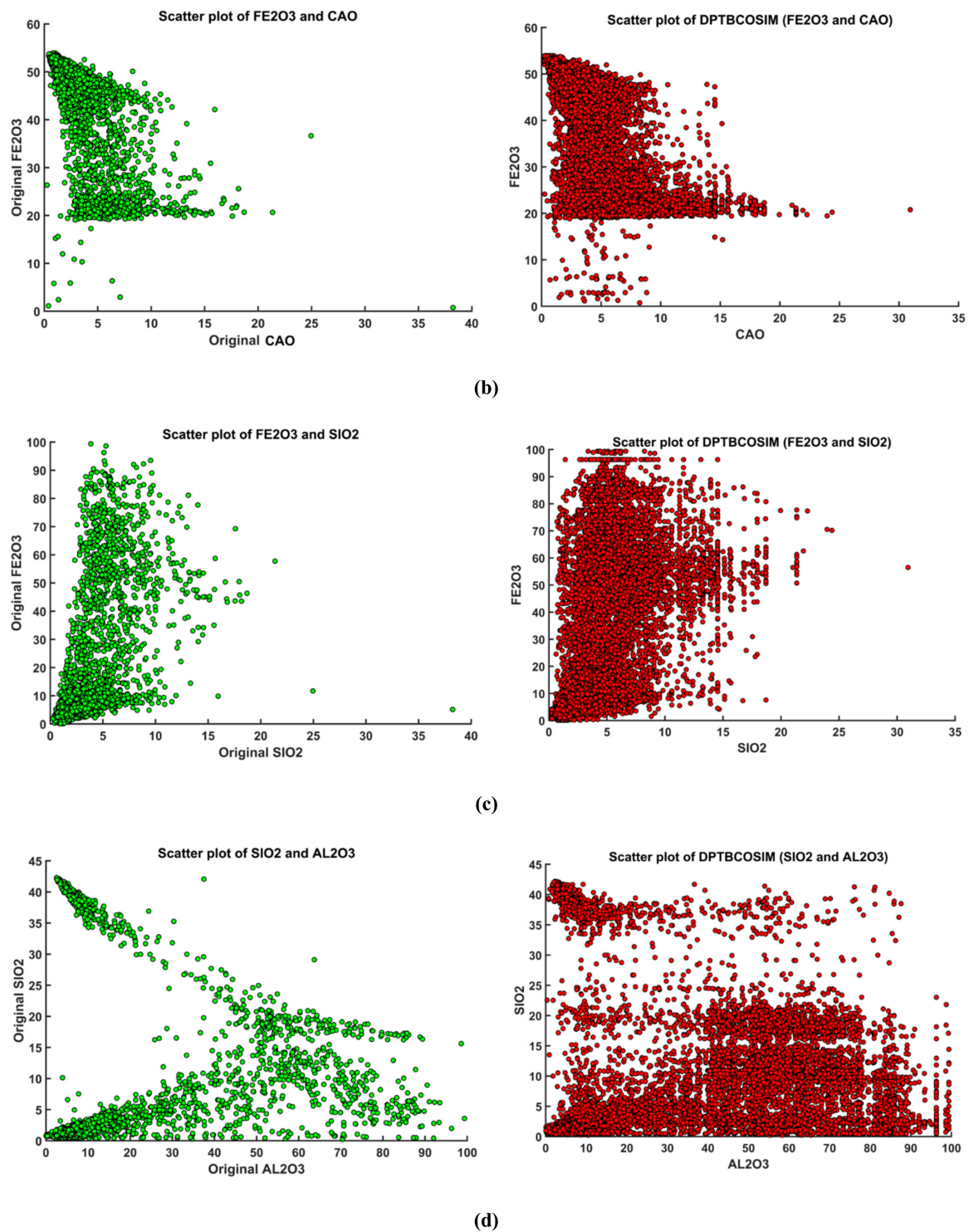


Figure 14. Cont.

Figure 14. *Cont.*

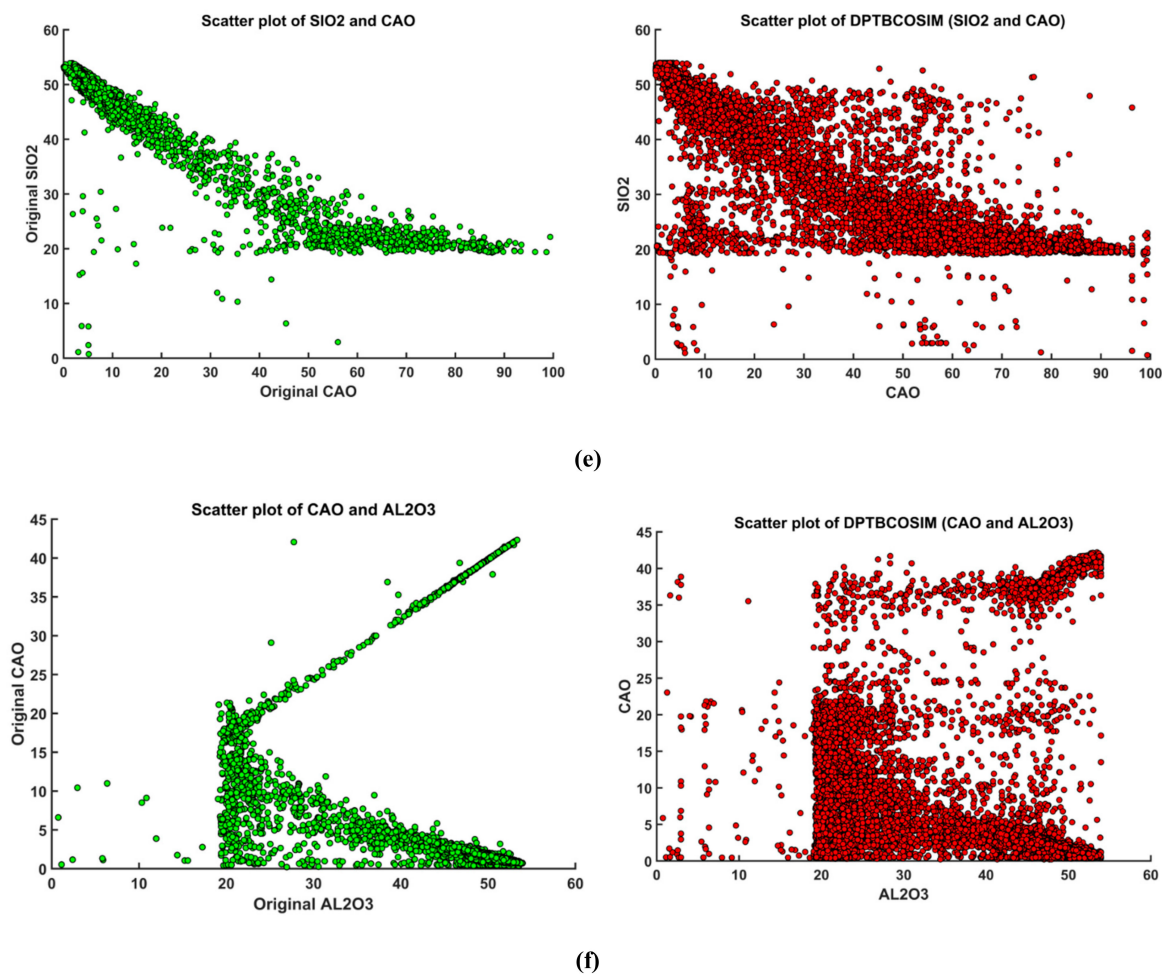


Figure 14. Reproduction of original correlation coefficient (green) between (a) Fe₂O₃ and Al₂O₃, (b) Fe₂O₃ and CaO, (c) Fe₂O₃ and SiO₂, (d) SiO₂ and Al₂O₃, (e) SiO₂ and CaO, (f) CaO and Al₂O₃ by PPMT method (red).

3.6. Mineral Resource Classification

Based on the JORC code definition (www.JORC.org), mineral resources can be classified into measured, indicated, or inferred based on the level of confidence. In fact, the guideline in this code was developed to assure transparency for investors in the declaration of mineral resources in order to prevent fraud [41]. A measured mineral resource is part of a deposit that presents a high level of confidence in the estimation of recovery functions such as tonnage, mean grade, and metal quantity above cutoff. Indicated mineral resources can be assigned to those areas that demonstrate a reasonable level of confidence in the estimation of recovery functions such as tonnage, mean grade, and metal quantity above the cutoff. Inferred mineral resources represent locations for which the recovery functions are evaluated at a low level of confidence. In this regard, there are mainly two algorithms for mineral resource classification, connected with either deterministic or stochastic paradigms. In the latter, one needs to employ, for instance, geostatistical simulation techniques to produce different scenarios of a mine deposit (i.e., realizations) with the aim of quantifying the uncertainty. This leads to probabilistic reporting of the mineral resource measures.

Mineral resource classification in this limestone deposit is done on the basis of two main targets, following the stochastic approach. One is related to classification based on ore zone definition (geological), in which mostly CaO and Fe₂O₃ are two critical components for the underlying zone. The second is mainly concerned with mining excavation units where CaO, SiO₂, and Al₂O₃ are vital variables for this zone definition. In the following, we present the results for both types of

mineral resource classification that define the different categories based on ore zone definitions and mining units.

3.6.1. Ore Zone Definitions

One of the main objectives of this study is to employ the proposed algorithm based on a combination of PPMT transformation and co-simulation algorithm, and to show the results of mineral resource classification by demonstrating their distinctions. As shown previously in the section on validating simulation results with regard to reproducing original mean, variance, correlation coefficient, and shape of bivariate relations between pairs of variables, the PPMT and co-simulation methodology corroborates that the outputs of realizations are statistically sound and can be applied for further processing, such as mineral resource classification. Aktas-South deposit is grouped into three main ore zones based on the definitions of chemical cutoffs as indicated in Table 4. CaO in this limestone deposit is the main chemical compound. Resource estimation of this variable based on JORC code is shown in Table 5 for each ore zone. In order to show the distinctions between outputs of resource classification of CaO (measured, indicated, inferred, and total tonnage), the results are constructed in one unique graph, shown in Figure 15. As previously explained, the classification of resources is modelled according to uncertainty, in which measured resources are quantified 90% of the time within $\pm 15\%$, indicated resources within $\pm 15\%$ and $\pm 30\%$, and inferred resources within $\pm 30\%$ and $\pm 100\%$, while other materials within more than $\pm 100\%$ are not distinguished as resources [41].

Table 4. Ore zone definitions based on chemical cutoffs.

Zone	Chemical Cutoffs
Marl-chert	$\leq 40\%$ and $\geq 20\%$ of CaO
Pale yellow limestone	$> 40\%$ of CaO and $< 3\%$ of Fe_2O_3
Brown limestone	$> 40\%$ of CaO and $\geq 3\%$ and $< 4.5\%$ of Fe_2O_3

Table 5. Resource estimation of CaO in Mt based on ore zone definitions.

Classification	Marl-Chert (Mt)	Pale Yellow Limestone (Mt)	Brown Limestone (Mt)
Measured	53	102.14288	52.56608
Indicated	30	10.79	5.4357
Inferred	125	67.99632	33.652
Total	208	180.9292	91.65378

As can be observed from Figure 15, marl-chert has the highest total tonnage of CaO, 208 Mt, according to the PPMT co-simulation method (proposed algorithm), followed by pale yellow limestone and brown limestone, with 181 Mt and 92 Mt, respectively. In the measured category, marl-chert ore and brown limestone ore tonnage are almost the same, 53 Mt, while pale yellow limestone has higher tonnage, 102 Mt. In the indicated and inferred categories, marl-chert has higher tonnages, 30 Mt and 125 Mt, respectively, followed by pale yellow limestone, 11 and 68 Mt, respectively, and brown limestone has the lowest tonnages, 5.5 Mt and 34 Mt, respectively. It should be mentioned that ore zone definition in this step has two restrictions (chemical cut-offs), and because of that results of resource classification differ.

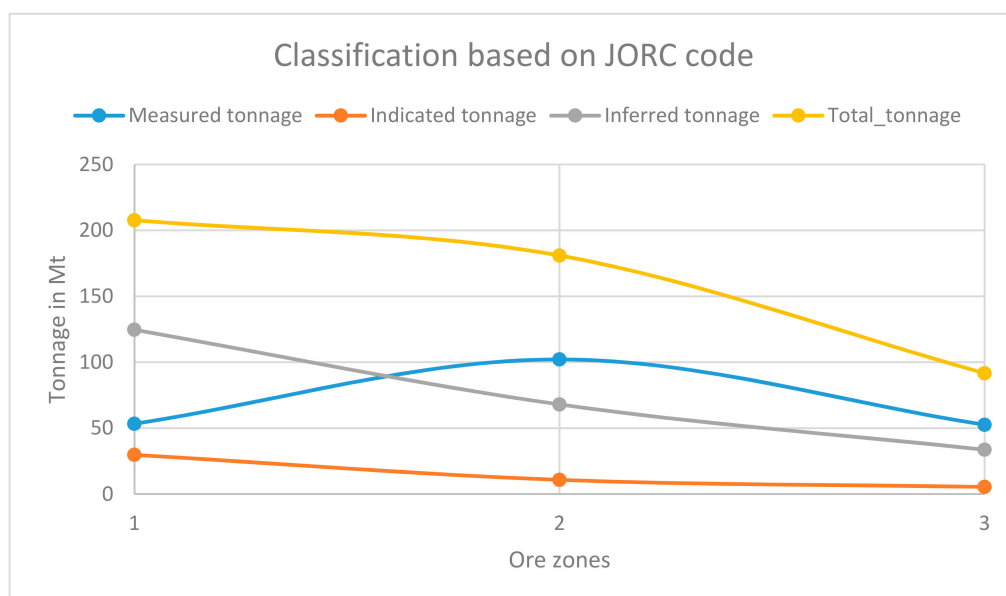


Figure 15. Resource classification of CaO in different ore zones: 1: marl-chert; 2: pale yellow limestone; 3: brown limestone.

3.6.2. Mining Units

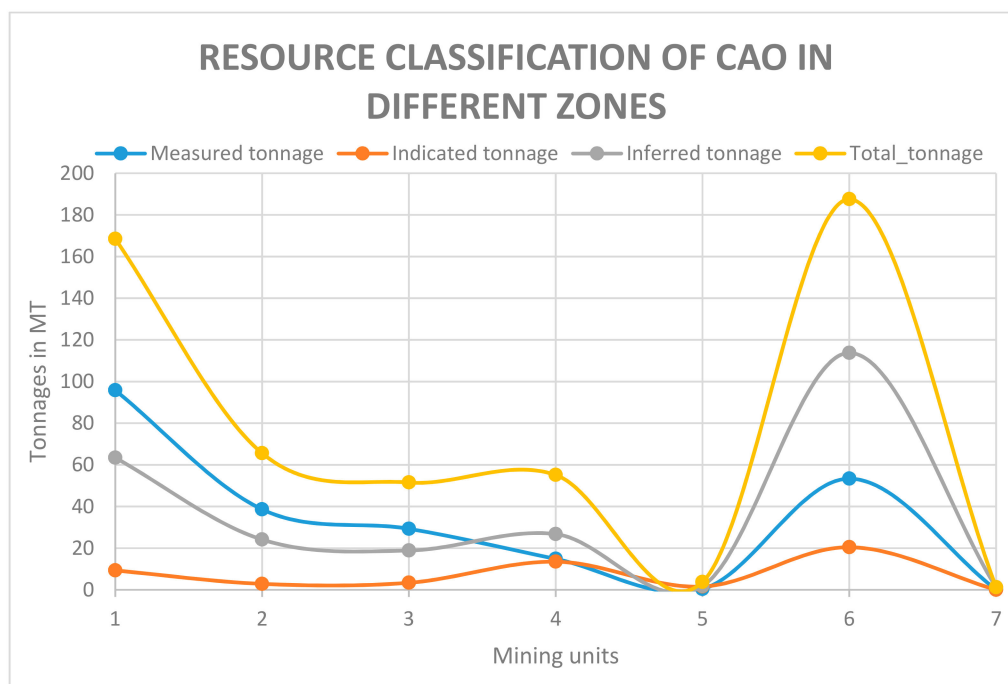
In this deposit, there is another classification based on chemical cutoff definitions, but this time from the mining destination perspective, whereas the previous tonnage classification was based on the definitions of ore zones in favor of geological interpretations. The definitions of these mining units are presented in Table 6. In this paradigm, the units are mainly established in accordance with three main chemical compounds, CaO, SiO₂, and Fe₂O₃. As also shown in Table 3, there is strong correlation among these three variables. The results of the proposed approach, in fact, show that the correlation coefficients are reproduced at a satisfactory level of confidence. The importance of this is shown in this section; for instance, these three variables are the key factors in favor of grouping the Aktas-South limestone deposit for mining excavation, which consequently impacts the rigorous classification of mineral resources. The list of mining units based on chemical cutoffs is shown in Table 6. It should be mentioned that in this classification, the number of restrictions (chemical cutoffs) reaches four, which means that the results of classification will be according to seven restrictions. As can be seen, CaO and SiO₂ are two chemical compounds that define the ore/waste classification technique. The tonnage for each classification based on JORC code in this deposit is summarized in Table 7, and all results of the mentioned method with resource classification are summarized in single graphs for highly green limestone (HGLS), brown limestone (BROWNLS), ferrous limestone (FEROLS), cherty limestone (CHERTYLS), cherty limestone 2 (CHERTYLS2), MARL, and WASTE in Figure 16, following the same method as explained in the previous section [41].

Table 6. Mining units with restriction in chemical characteristics.

Mining Unit	Chemical Cutoffs
HGLS	$\text{CaO} \geq 40$ and $\text{SiO}_2 \leq 15$ and $\text{Fe}_2\text{O}_3 < 3$
BROWNLS	$\text{CaO} \geq 40$ and $\text{SiO}_2 \leq 15$ and $\text{Fe}_2\text{O}_3 \geq 3$ and $\text{Fe}_2\text{O}_3 < 4$
FEROLS	$\text{CaO} \geq 40$ and $\text{SiO}_2 \leq 15$ and $\text{Fe}_2\text{O}_3 \geq 4$
CHERTYLS	$\text{CaO} < 50$ and $\text{CaO} > 20$ and $\text{SiO}_2 > 15$ and $\text{SiO}_2 \leq 40$
CHERTYLS2	$\text{CaO} < 40$ and $\text{CaO} > 30$ and $\text{SiO}_2 \leq 15$
MARL	$\text{CaO} < 45$ and $\text{CaO} > 10$ and $\text{SiO}_2 > 40$
WASTE	$\text{CaO} \leq 10$ and $\text{CaO} > 0$ and $\text{SiO}_2 > 40$

Table 7. Resource estimation of CaO in Mt based on mining unit.

Category	HGLS	BROWNLS	FEROLS	CHERTYLS	CHERTYLS2	MARL	WASTE
Measured tonnage	95.8	38.6	29.3	14.9	0.4	53.4	0.0
Indicated tonnage	9.3	2.8	3.4	13.5	1.5	20.4	0.0
Inferred tonnage	63.4	24.1	18.9	26.8	1.8	113.8	1.2
Total tonnage	168.5	65.6	51.5	55.1	3.7	187.5	1.2

**Figure 16.** Resource classification of CaO in different mining units: 1: HGLS; 2: BROWNLS; 3: FEROLS; 4: CHERTYLS; 5: CHERTYLS2; 6: MARL; 7: WASTE.

Depending on the chemical restrictions of each lithology, resource tonnages have different trends of results by category. The highest total tonnages are shown in HGLS and MARL, followed by almost the same tonnages in BROWNS, FEROLS, and CHERTYLS (see Figure 16). The lowest total tonnages are computed in CHERTYLS2 and WASTE. Turning to the measured category, the highest tonnage is seen in HGLS, followed by MARL, BROWNS, FEROLS, and CHERTYLS, and the lowest tonnages are reported in CHERTYLS and WASTE. With an increased number of geological restrictions, the results of resource classification change more chaotically. However, it is clearly shown that CHERTYLS2 and WASTE, which have narrow restrictions in CaO, have the lowest tonnages in every category.

4. Conclusions

This contribution provides a technique for the multivariate geostatistical analysis of co-regionalized variables, particularly for datasets where complexity exists between bivariate relationships. The proposed algorithm in this study is based on the combination of a conventional stochastic simulation approach (Gaussian (co)-simulation) and a recently developed factorization technique (projection pursuit multivariate transformation (PPMT)). A main difference from other multivariate geostatistical approaches is that in PPMT, there is no need to further transform the factors to remove the correlation. Instead, a linear model of co-regionalization should be defined to introduce the small cross-spatial dependency among the transformed variables, in which it can be inferred from the factors right after PPMT forward transformation.

In addition, the real case study, limestone deposit, illustrates the effectiveness of the proposed algorithm for mineral resource classification based on the two-zone separation following the JORC

code definition. To do so, the outputs of the realizations are first examined to determine whether they are statistically valid, then taken into account to classify resources as measured, inferred, or indicated. Through the validation step, reproduction of mean, variance, and global (cross)-correlation is examined, illustrating that all simulation results, on average, converge to the original statistical parameter, indicating the robustness of the proposed algorithm. Behind the seeming simplicity and great number of practical investigations, much effort is still needed to deal with more complex sampling configuration, particularly in the presence of partially or heterotopic sampling patterns. In such cases, using PPMT is restricted and an imputation technique may be an alternative to combine PPMT with (co)-simulation.

Author Contributions: N.B. implemented the experiments and wrote the paper, and N.M. wrote and reviewed the paper.

Funding: This research was funded by NAZARBAYEV UNIVERSITY via Faculty Development Competitive Research Grants for 2018–2020, grant number 090118FD5336.

Acknowledgments: The authors thank the Datamine Company for providing the dataset of limestone deposit for the underlying case study. We deeply thank Paul Alexandre, the two anonymous reviewers, and editorial board for their invaluable efforts towards improving the overall scientific quality of this manuscript.

Conflicts of Interest: The authors declare no conflict of interest. The founding sponsors had no role in the design of the study; in the collection, analyses, or interpretation of data; in the writing of the manuscript, and in the decision to publish the results.

References

1. Dimitrakopoulos, R. Stochastic Mine Planning—Methods, Examples and Value in an Uncertain World. In *Advances in Applied Strategic Mine Planning*; Springer: Cham, Switzerland, 2018; pp. 101–115.
2. Hustrulid, W.A.; Kuchta, M.; Martin, R.K. *Open Pit Mine Planning and Design, Two Volume Set & CD-ROM Pack: V1: Fundamentals, V2: CSMine Software Package, CD-ROM: CS Mine Software*; CRC Press: Boca Raton, FL, USA, 2013.
3. Kasmaee, S.; Raspa, G.; De Fouquet, C.; Tinti, F.; Bonduà, S.; Bruno, R. Geostatistical Estimation of Multi-Domain Deposits with Transitional Boundaries: A Sensitivity Study for the Sechahun Iron Mine. *Minerals* **2019**, *9*, 115. [[CrossRef](#)]
4. Joint Ore Reserves Committee (JORC) Code. The JORC Code and Guidelines. In *Australasian Code for Reporting of Exploration Results, Mineral Resources and Ore Reserves Prepared by The Australasian Institute of Mining and Metallurgy (AusIMM)*; Australian Institute of Geoscientists and Minerals Council of Australia: Crows Nest, Australia, 2012; Available online: www.jorc.org (accessed on 7 October 2015).
5. Monkhouse, P.H.L.; Yeates, G.A. Beyond Naïve Optimisation. In *Advances in Applied Strategic Mine Planning*; Springer: Cham, Switzerland, 2018; pp. 3–18.
6. Mai, N.L.; Erten, O.; Topal, E. A new generic open pit mine planning process with risk assessment ability. *Int. J. Coal Sci. Technol.* **2016**, *3*, 407–417. [[CrossRef](#)]
7. Dimitrakopoulos, R. Stochastic optimization for strategic mine planning: A decade of developments. *J. Min. Sci.* **2011**, *47*, 138–150. [[CrossRef](#)]
8. Khosrowshahi, S.; Shaw, W.J.; Yeates, G.A. Quantification of Risk Using Simulation of the Chain of Mining—Case Study at Escondida Copper, Chile. In *Advances in Applied Strategic Mine Planning*; Springer: Cham, Switzerland, 2018; pp. 57–74.
9. Vallejo, M.N.; Dimitrakopoulos, R. Stochastic orebody modelling and stochastic long-term production scheduling at the KéMag iron ore deposit, Quebec, Canada. *Int. J. Mining Reclam. Environ.* **2018**, *33*, 462–479. [[CrossRef](#)]
10. Benndorf, J.; Dimitrakopoulos, R. Stochastic long-term production scheduling of iron ore deposits: Integrating joint multi-element geological uncertainty. *J. Min. Sci.* **2013**, *49*, 68–81. [[CrossRef](#)]
11. De-Vitry, C.; Vann, J.; Arvidson, H. Multivariate iron ore deposit resource estimation—A practitioner’s guide to selecting methods. *Appl. Earth Sci.* **2010**, *119*, 154–165. [[CrossRef](#)]
12. Dimitrakopoulos, R.; Farrelly, C.T.; Godoy, M. Moving forward from traditional optimization: Grade uncertainty and risk effects in open-pit design. *Min. Technol.* **2002**, *111*, 82–88. [[CrossRef](#)]
13. Menabde, M.; Froyland, G.; Stone, P.; Yeates, G.A. Mining Schedule Optimisation for Conditionally Simulated Orebodies. In *Advances in Applied Strategic Mine Planning*; Springer: Cham, Switzerland, 2018; pp. 91–100.

14. Dimitrakopoulos, R. Conditional simulation algorithms for modelling orebody uncertainty in open pit optimisation. *Int. J. Surf. Min. Reclam. Environ.* **1998**, *12*, 173–179. [CrossRef]
15. Emery, X.; Lantuejoul, C. Tbsim: A computer program for conditional simulation of three-dimensional gaussian random fields via the turning bands method. *Comput. Geosci.* **2006**, *32*, 1615–1628. [CrossRef]
16. Isaaks, E.H. The Application of Monte Carlo Methods to the Analysis of Spatially Correlated Data: Unpublished. Ph.D. Thesis, Stanford University, Stanford, CA, USA, 1999; 213p.
17. Journel, A.G. Modeling Uncertainty: Some Conceptual Thoughts. In *Geostatistics Valencia 2016*; Springer: Cham, Switzerland, 1994; Volume 6, pp. 30–43.
18. Boisvert, J.B.; Rossi, M.E.; Ehrig, K.; Deutsch, C.V. Geometallurgical Modeling at Olympic Dam Mine, South Australia. *Math. Geosci.* **2013**, *45*, 901–925. [CrossRef]
19. Deutsch, C.V. Geostatistical Modelling of Geometallurgical Variables—Problems and Solutions. In Proceedings of the Second AUSIMM International Geometallurgy Conference/Brisbane, Brisbane, Australia, 30 September 2013; Volume 30, pp. 7–15.
20. Leuangthong, O.; Deutsch, C.V. Stepwise Conditional Transformation for Simulation of Multiple Variables. *Math. Geosci.* **2003**, *35*, 155–173.
21. Van den Boogaart, K.G.; Mueller, U.; Tolosana-Delgado, R. An affine equivariant multivariate normal score transform for compositional data. *Math. Geosci.* **2017**, *49*, 231–251. [CrossRef]
22. Barnett, R.; Manchuk, J.; Deutsch, C. Projection pursuit multivariate transform. *Math. Geosci.* **2014**, *46*, 337–359. [CrossRef]
23. Barnett, R.M.; Manchuk, J.G.; Deutsch, C.V. The Projection-Pursuit Multivariate Transform for Improved Continuous Variable Modeling. *SPE J.* **2016**, *21*, 2010–2026. [CrossRef]
24. Battalgazy, N.; Madani, N. Categorization of Mineral Resources Based on Different Geostatistical Simulation Algorithms: A Case Study from an Iron Ore Deposit. *Nat. Resour. Res.* **2019**, *28*, 1329–1351. [CrossRef]
25. Adeli, A.; Emery, X.; Dowd, P. Geological Modelling and Validation of Geological Interpretations via Simulation and Classification of Quantitative Covariates. *Minerals* **2017**, *8*, 7. [CrossRef]
26. Shao, H.; Sun, X.; Wang, H.; Zhang, X.; Xiang, Z.; Tan, R.; Chen, X.; Xian, W.; Qi, J. A method to the impact assessment of the returning grazing land to grassland project on regional eco-environmental vulnerability. *Environ. Impact Assess. Rev.* **2017**, *56*, 155–167. [CrossRef]
27. Vasylichuk, Y.V.; Deutsch, C.V. Improved grade control in open pit mines. *Min. Technol.* **2018**, *127*, 84–91. [CrossRef]
28. Rivoirard, J. *Introduction to Disjunctive Kriging and Non-Linear Geostatistics*; Clarendon Press: Oxford, UK, 1994; 181p.
29. Deutsch, C.V.; Journel, A.G. *GSLIB: Geostatistical Software Library and User's Guide*, 2nd ed.; Oxford University Press: New York, NY, USA, 1998.
30. Journel, A.G.; Huijbregts, C.J. *Mining Geostatistics*; Academic Press: London, UK, 1978.
31. Barnett, R.M. Projection Pursuit Multivariate Transform. In *Geostatistics Lessons*; Deutsch, J.L., Ed.; Centre for Computational Geostatistics, Department of Civil and Environmental Engineering, University of Alberta: Edmonton, AB, Canada, 2017; Available online: <http://www.geostatisticslessons.com/lessons/lineardecorrelation.html> (accessed on 24 October 2018).
32. Reed, M.; Simon, B. *Methods of Modern Mathematical Physics. I, II, III, IV*; Academic Press Inc.: New York, NY, USA, 1972; Volume 1975, p. 1979.
33. Emery, X. A turning bands program for conditional co-simulation of cross-correlated Gaussian random fields. *Comput. Geosci.* **2008**, *34*, 1850–1862. [CrossRef]
34. Verly, G.W. Sequential Gaussian Cosimulation: A Simulation Method Integrating Several Types of Information. In *Geostatistics Valencia 2016*; Springer: Cham, Switzerland, 1993; Volume 5, pp. 543–554.
35. Abildin, Y.; Madani, N.; Topal, E. A Hybrid Approach for Joint Simulation of Geometallurgical Variables with Inequality Constraint. *Minerals* **2019**, *9*, 24. [CrossRef]
36. Wackernagel, H. *Multivariate Geostatistics: An Introduction with Applications*; Springer: Berlin/Heidelberg, Germany, 2003.
37. Rivoirard, J.; Demange, C.; Freulon, X.; Lécureuil, A.; Bellot, N. A top-cut model for deposits with heavy-tailed grade distribution. *Math. Geosci.* **2013**, *45*, 967–982. [CrossRef]
38. Maleki, M.; Madani, N.; Emery, X. Capping and kriging grades with long-tailed distributions. *J. South. Afr. Inst. Min. Metall.* **2014**, *114*, 255–263.

39. Sinclair, A.J.; Blackwell, G.H. *Applied Mineral Inventory Estimation*; Cambridge University Press (CUP): Cambridge, UK, 2002.
40. Deutsch, J.L.; Deutsch, C.V. *Some Geostatistical Software Implementation Details*; Centre for Computational Geostatistics, University of Alberta: Edmonton, AB, Canada, 2010; Volume 412.
41. Rossi, M.E.; Deutsch, C.V. *Mineral Resource Estimation*; Springer: Berlin, Germany, 2014.
42. Madani, N.; Yagiz, S.; Adoko, A.C. Spatial Mapping of the Rock Quality Designation Using Multi-Gaussian Kriging Method. *Minerals* **2018**, *8*, 530. [[CrossRef](#)]
43. Goovaerts, P. *Geostatistics for Natural Resources Evaluation*; Oxford University Press: New York, NY, USA, 1997.
44. Leuangthong, O.; Khan, K.D.; Deutsch, C.V. *Solved Problems in Geostatistics*; John Wiley & Sons: Hoboken, NJ, USA, 2011.
45. Emery, X. Iterative algorithms for fitting a linear model of coregionalization. *Comput. Geosci.* **2010**, *36*, 1150–1160. [[CrossRef](#)]
46. Maleki, M.; Emery, X.; Mery, N. Indicator Variograms as an Aid for Geological Interpretation and Modeling of Ore Deposits. *Minerals* **2017**, *7*, 241. [[CrossRef](#)]
47. Paravarzar, S.; Emery, X.; Madani, N. Comparing sequential Gaussian simulation and turning bands algorithms for cosimulating grades in multi-element deposits. *Comptes Rendus Geosci.* **2015**, *347*, 84–93. [[CrossRef](#)]
48. Madani, N.; Emery, X. A comparison of search strategies to design the cokriging neighborhood for predicting coregionalized variables. *Stoch. Environ. Res. Risk Assess.* **2019**, *33*, 183–199. [[CrossRef](#)]
49. Lantuejoul, C. *Geostatistical Simulation, Models and Algorithms*; Springer: Berlin, Germany, 2002.
50. Madani, N.; Carranza, E.J.M. Co-simulated Size Number: An Elegant Novel Algorithm for Identification of Multivariate Geochemical Anomalies. *Nat. Resour. Res.* **2019**, in press. [[CrossRef](#)]
51. Eze, P.N.; Madani, N.; Adoko, A.C. Multivariate mapping of heavy metals spatial contamination in a Cu–Ni exploration field (Botswana) using turning bands co-simulation algorithm. *Nat. Resour. Res.* **2019**, *28*, 109–124. [[CrossRef](#)]
52. Madani, N. Multi-located cokriging: An application to grade estimation in the mining industry. In *Mining Goes Digital*; CRC Press: Wroclaw, Poland, 2019; pp. 158–167.
53. Maleki, M.; Madani, N. Multivariate geostatistical analysis: An application to ore body evaluation. *Iranian J. Earth Sci.* **2017**, *8*, 173–184.



© 2019 by the authors. Licensee MDPI, Basel, Switzerland. This article is an open access article distributed under the terms and conditions of the Creative Commons Attribution (CC BY) license (<http://creativecommons.org/licenses/by/4.0/>).